AGU ADVANCING EARTH AND SPACE SCIENCES

JGR Atmospheres

RESEARCH ARTICLE
10.1029/2025JD046229

Disentangling Anthropogenic Effects on Southern Hemisphere Circulation and Surface Climate: A Multi-Model Large Ensemble Approach

Leandro B. Díaz[1,2,3], Amy H. Butler[4], David Avisar[5,6], Sabine Bischof[7], Chloe L. Boehm[8], Ghyslaine Boschat[9,10], William J. Dow[11], Chaim I. Garfinkel[5], Kevin M. Grise[12], Hemant Khatri[13], Bianca Mezzina[14], Marisol Osman[1,2,3], Jonathon S. Wright[15], Panos J. Athanasiadis[16], Julie M. Arblaster[10,17], Erik Behrens[18], Thomas J. Bracegirdle[19], Yuanrui Chen[15], Eun-Pa Lim[9,10], Amanda C. Maycock[11], Seung-Ki Min[20], Julia Mindlin[21], Scott M. Osprey[22,23], Michael Sigmond[24], Doug Smith[13], and Tiffany Shaw[25]

[1]Universidad de Buenos Aires, Facultad de Ciencias Exactas y Naturales, Departamento de Ciencias de la Atmósfera y los Océanos (DCAO), Buenos Aires, Argentina, Buenos Aires, Argentina, [2]CONICET – Universidad de Buenos Aires. Centro de Investigaciones del Mar y la Atmósfera (CIMA), Buenos Aires, Argentina, [3]Instituto Franco-Argentino de Estudios sobre el Clima y sus Impactos (IFAECI) – IRL 3351 – CNRS-CONICET-IRD-UBA, Buenos Aires, Argentina, [4]NOAA Chemical Sciences Laboratory, Boulder, CO, USA, [5]Fredy & Nadine Herrmann Institute of Earth Sciences, The Hebrew University of Jerusalem, Jerusalem, Israel, [6]The Department of Applied Mathematics, Israel Institute for Biological Research, Ness-Ziona, Israel, [7]GEOMAR Helmholtz Centre for Ocean Research Kiel, Kiel, Germany, [8]Department of Atmospheric Science, Colorado State University, Fort Collins, CO, USA, [9]Bureau of Meteorology, Melbourne, VIC, Australia, [10]ARC Special Research Initiative for Securing Antarctica's Environmental Future, Clayton, VIC, Australia, [11]School of Earth and Environment, University of Leeds, Leeds, UK, [12]Department of Environmental Sciences, University of Virginia, Charlottesville, VA, USA, [13]Met Office Hadley Centre, Exeter, UK, [14]Earth and Climate Research Center, Earth and Life Institute, Université catholique de Louvain, Louvain-la-Neuve, Belgium, [15]Department of Earth System Science, Institute for Global Change Studies, Ministry of Education Key Laboratory for Earth System Modeling, Tsinghua University, Beijing, China, [16]CMCC Foundation - Euro-Mediterranean Center on Climate Change, Bologna, Italy, [17]School of Earth, Atmosphere and Environment, Monash University, Clayton, VIC, Australia, [18]Earth Sciences New Zealand, Wellington, New Zealand, [19]British Antarctic Survey, Cambridge, UK, [20]Division of Environmental Science and Engineering, Pohang University of Science and Technology, Pohang, South Korea, [21]Leipzig University, Leipzig, Germany, [22]National Centre for Atmospheric Science, University of Oxford, Oxford, UK, [23]Atmospheric, Oceanic and Planetary Physics, University of Oxford, Oxford, UK, [24]Canadian Centre for Climate Modelling and Analysis, Environment and Climate Change Canada, Victoria, BC, Canada, [25]The University of Chicago, Chicago, IL, USA

Leandro B. Díaz and Amy H. Butler contributed equally to this work.

Key Points:

- Greenhouse gases drive Southern Hemisphere circulation changes year-round, while ozone is a key driver during austral spring and summer
- Although weaker, anthropogenic aerosol effects are substantial and should be accounted for in attribution studies
- Persistent model-observational discrepancies exist for recent trends in Southern Ocean sea surface temperature and sea ice extent

Supporting Information:

Supporting Information may be found in the online version of this article.

Correspondence to:

A. H. Butler,
amy.butler@noaa.gov

Citation:

Díaz, L. B., Butler, A. H., Avisar, D., Bischof, S., Boehm, C. L., Boschat, G., et al. (2026). Disentangling anthropogenic effects on Southern Hemisphere circulation and surface climate: A multi-model large ensemble approach. *Journal of Geophysical Research: Atmospheres*, *131*, e2025JD046229. https://doi.org/10.1029/2025JD046229

Received 23 DEC 2025
Accepted 6 JUL 2026

Abstract Southern Hemisphere (SH) circulation and surface climate changes are emerging in recent decades. For example, in most seasons, the SH Hadley cell edge and the eddy-driven jet stream have shifted polewards, and the Southern Annular Mode (SAM) has trended towards its positive phase. However, attributing these changes to specific external forcings, such as greenhouse gas (GHG) increases or stratospheric ozone depletion, has been hindered by small ensemble sizes and lack of coherent forcing methodology across multiple models. In this study, we analyzed simulations from 10 models within the Large Ensemble Single Forcing Model Intercomparison Project (LESFMIP) to isolate the long-term (1850–2014) SH climate response to individual forcings (GHGs, aerosols, and ozone). We found that long-term SH climate trends are dominated by GHGs across all seasons. Over this time period, stratospheric ozone depletion exerts an influence comparable to GHGs but is restricted to austral spring and summer. Although anthropogenic aerosols show weaker effects on climate trends that oppose those induced by GHG forcing and ozone depletion, they have a noticeable impact. Notably, ozone recovery following the Montreal Protocol is currently weakening or reversing spring and summer trends in key circulation metrics. Finally, we quantify the degree to which the observed sea surface cooling of the Southern Ocean and Antarctic sea ice increase from 1980 to 2014 fall outside the models' ensemble spread. Our results highlight the need to better understand the roles of different forcings, model differences, and discrepancies between models and observations to constrain projections of future Southern Hemisphere climate change.

Plain Language Summary Atmospheric and oceanic circulation changes are emerging in the Southern Hemisphere (SH). To better understand the drivers of these changes, in this study we use a new multi-model large ensemble data set to look at how specific factors (forcings) have individually influenced the long-

term SH climate trends from 1850 to 2014. We find that greenhouse gases are the main driver of long-term changes in the SH since the preindustrial era. The impact of stratospheric ozone depletion is comparable to greenhouse gases, but only during austral spring and summer. On the other hand, anthropogenic aerosols partially counteract greenhouse gas effects on the circulation. The models are able to simulate the recent weakening or even reversal of some of the trends in key atmospheric circulation metrics due to the recovery of the ozone layer following the enactment of the Montreal Protocol and its amendments. However, the disagreement between model simulations and real-world observations for recent trends in Southern Ocean sea surface temperatures and Antarctic sea ice highlights the need for more research to reliably project future climate change in this crucial region.

1. Introduction

The global climate has undergone significant changes in recent decades due to anthropogenic activities. The circulation and surface climate of the Southern Hemisphere (SH) is no exception, with observation-based studies reporting various emerging signals associated with climate change (Gulev et al., 2021; Shaw et al., 2024). Key observed trends include a poleward expansion of the Southern Hadley Cell (Grise & Davis, 2020; Johanson & Fu, 2009; Lionello et al., 2024; Min & Son, 2013), a positive trend in the austral summer Southern Annular Mode (SAM, Fogt & Marshall, 2020; Purich et al., 2026), a poleward shift of the austral summer SH eddy-driven jet (Mindlin et al., 2025; Woollings et al., 2023), including near-surface extreme wind (Chou et al., 2025), and a strengthening of the storm tracks (Chemke et al., 2022; Shaw et al., 2022). The Southern Ocean heat content has experienced an accelerated increase in recent decades (Auger et al., 2021; Cai et al., 2023; Shi et al., 2021). Antarctic sea ice slightly increased between 1979 and 2015, but has experienced a rapid decline in recent years (Eayrs et al., 2021; Parkinson, 2019; Purich & Doddridge, 2023). A wetting trend has also been evidenced in SH land monsoon areas (Cao et al., 2023), with regions like Southeastern South America and northern Australia standing out for their positive austral summer trend (Díaz et al., 2021; Heidemann et al., 2023; Varuolo-Clarke et al., 2021). Conversely, SH semi-arid regions—such as southern Chile, southern Africa, and south Australia—have experienced a drying trend during austral autumn and winter (Boisier et al., 2018; Cai & Cowan, 2013; Cai et al., 2012; McKay et al., 2023; Purich et al., 2013; Timbal & Drosdowsky, 2013).

A major challenge in attributing observed SH climate changes and projecting their future evolution is disentangling and understanding the role of various external forcings. The most prominent of these are increasing greenhouse gas (GHG) concentrations and changes in stratospheric ozone. Global GHG concentrations have risen at high rates since the mid-20th century, primarily due to the widespread use of fossil fuels (IPCC, 2021). In contrast, the Antarctic stratospheric ozone layer experienced significant depletion in the late 20th century because of manmade ozone-depleting substances (ODS) such as chlorofluorocarbons. Actions agreed upon in the Montreal Protocol and its amendments to substantially reduce ODS emissions are expected to lead to Antarctic ozone recovery by the mid-to-late 21st century (e.g., Keeble et al., 2021). Anthropogenic aerosols, which have a net global-mean cooling effect, peaked in the mid-1970s in Europe and North America but in the mid-2000s in Asia; and air quality policies have since resulted in global-mean aerosol decreases (Fiedler et al., 2019).

Pioneering studies suggested that Antarctic ozone depletion could largely explain the structure and sign of observed summertime SH climate trends in the last decades of the 20th century (Arblaster & Meehl, 2006; Gillett & Thompson, 2003; Thompson et al., 2011; Thompson & Solomon, 2002). Ozone depletion has led to a later seasonal dissipation of the stratospheric polar vortex (the "final stratospheric warming" or FSW; Byrne & Shepherd, 2018). This delay in the stratospheric seasonal cycle propagates downward and delays the seasonal timing of the equatorward shift of the eddy-driven jet stream, resulting in an anomalous poleward shift of the eddy-driven jet and positive phase of the SAM (Butler & Domeisen, 2021; Byrne & Shepherd, 2018; Saggioro & Shepherd, 2019). Single forcing simulations confirm that ozone depletion is the main driver of the observed poleward shift of the SH jet stream in summertime (McLandress et al., 2011; Morgenstern, 2021; Polvani et al., 2011; Purich et al., 2026; Waugh et al., 2015). Furthermore, stratospheric ozone depletion has significantly contributed to the observed austral summer Hadley Cell widening—an effect that is distinguishable from other external forcings like GHG increases (Grise et al., 2019; Kim et al., 2017; Min & Son, 2013). This widening further contributes to the poleward shift of the SH eddy-driven jet and extratropical storm tracks (Grise et al., 2014; Son et al., 2009), as well as alterations in the shape and position of the South Pacific Convergence

Zone (Brönnimann et al., 2017). The poleward circulation shifts associated with ozone depletion altered precipitation patterns, leading to increases at high latitudes and decreases at mid-latitudes, which could connect to negative precipitation trends in southwestern South America in austral summer (Boisier et al., 2018). SH subtropical moistening during austral summer in late 20th-century, including observed positive trends in regions like southeastern South America, Australia and South Africa, has been attributed to ozone depletion as well (Gonzalez et al., 2014; Hendon et al., 2014; Kang et al., 2011). Finally, modelling studies have reported that ozone depletion can also alter the Southern Ocean circulation by inducing a poleward shift of the surface wind stress, which strengthens the subpolar meridional overturning (Sigmond et al., 2011; Solomon et al., 2015).

GHG increases have also been found in previous studies to contribute to observed changes in the SH circulation, with a signature that extends year round (Kushner et al., 2001; Shindell & Schmidt, 2004). These include: expansion of the SH Hadley Cell (Grise et al., 2019; Nguyen et al., 2015); positive SAM trend (Arblaster & Meehl, 2006; Boisier et al., 2018); a sea level pressure increase over the SH mid-latitudes and a decrease over the SH high latitudes (Gillett et al., 2013); SH mid-latitude drying and high-latitude moistening (Fyfe et al., 2012); negative precipitation trends in southwestern South America (Boisier et al., 2018; Vera & Díaz, 2015) and southwestern Australia (Delworth & Zeng, 2014), and positive precipitation trends in southeastern South America (Vera & Díaz, 2015; Zhang et al., 2016). Both ozone depletion and increasing GHGs have driven changes in the zonal-mean atmospheric circulation of the same sign, albeit with different seasonality and underlying mechanisms (Eyring et al., 2013; Son et al., 2018). However, since around 2000, stratospheric ozone has been recovering (Salby et al., 2011; Solomon et al., 2016). This means there is an inflection point in ozone forcing, while at the same time, GHG forcing has continued to increase. Some recent studies suggest that ozone recovery is already driving changes in the SH circulation that are opposite to those resulting from ozone depletion (Banerjee et al., 2020; Zambri et al., 2021; Zheng, 2024). Therefore, the future evolution of the SH summer jet stream and its related circulation is thought to be the result of a tug-of-war between increasing GHGs and ozone recovery (Arblaster et al., 2011; Karpechko et al., 2010; Perlwitz, 2011).

Although anthropogenic aerosol emissions have received less attention in relation to their impact on the SH climate, they are also an important forcing factor. Increased aerosols result in global cooling due to their radiative effect (e.g., Gillett et al., 2021), even though most anthropogenic aerosol emissions occur in the Northern Hemisphere (NH). This means radiative effects from increasing aerosols historically counteract those from increasing GHGs, both in terms of global temperature change and more regional climate and circulation changes (e.g., Xie et al., 2013). For example, the SH subtropical jet was shown to weaken under enhanced aerosol concentrations but strengthen in response to GHGs (Rotstayn et al., 2013; Wang et al., 2020). However, it has also been suggested that changes in the zonal-mean circulation driven by aerosol forcing do not universally mirror those due to GHG forcing (Choi et al., 2019; Wang et al., 2020). Moreover, the global mean trend of aerosol forcing has reversed in recent decades due to changes in air quality policies that have reduced aerosol emissions (Quaas et al., 2022). For these reasons a more thorough investigation on how aerosols influence the SH circulation and where and when they oppose or amplify GHG-driven changes is necessary.

Despite significant advances over the last 20 years in attributing emerging climate signals in the SH, major challenges remain in understanding these changes and how they may evolve in the future. Firstly, while studies generally demonstrate that stratospheric ozone depletion plays a significant role in explaining late 20th century SH mid- and high-latitude climate trends, particularly in summer, as well as a year-round contribution from GHG forcing, the comparative role of each of these forcings is unclear and varies between studies. This is because the studies are based on different models or model ensembles, often with different forcing data sets (Eyring et al., 2013; Haase et al., 2020; Ivanciu et al., 2021; Morgenstern, 2021), and use different methodologies for comparison. Secondly, despite a clear indication of the role of ozone depletion in SH circulation and climate trends over the late 20th century, the amplitude of the response varies substantially across models. Thirdly, many of these studies are limited by the availability of multiple realizations for each experiment, particularly those related to ozone forcing. Long-term signals may contain components related to internal climate variability, so multiple realizations of each experiment are necessary to isolate the forced signals (Deser et al., 2020; Maher et al., 2021). Fourthly, the role of aerosol forcing has received much less attention than that of other anthropogenic forcings, such as GHG and ozone forcing. Consequently, the extent to which aerosol forcing contributes is more uncertain. Fifthly, the focus of most studies has been on changes during austral summer, when the observed signals are generally more prominent. However, the impact of climate change is relevant throughout the year. Some climate signals have the potential to emerge outside of the dynamically active seasons, during the transition seasons, so it is necessary to expand the scope to include other seasons as well (Shaw et al., 2024). Finally, the extent to which an ozone recovery signal could be identified in the circulation after 2000 has not yet been fully explored.

Additionally, though robust signals have emerged in the observations, some discrepancies with models persist (Shaw et al., 2024; Simpson et al., 2025). For example, high-latitude Southern Ocean sea surface temperatures (SSTs) decreased and Antarctic sea ice increased from 1979 to 2014, but the models instead show warming and sea ice loss over this period (Roach et al., 2023). The role of ozone forcing via the SAM over this time period has been heavily debated (e.g., Dong et al., 2023; Polvani et al., 2021; Seviour et al., 2019). More recently, Hartmann (2022) suggested that the La Niña-like trend in tropical SSTs over the observational record, which is not captured by models, may be related to ozone depletion, which was supported by a fully coupled model experiment (Dong et al., 2025). Resolving these discrepancies is limited by persistent model biases, but could be reduced through multi-model comparisons and large ensembles to separate the forced response from internal variability.

The objective of this study is to use simulations from the recently generated Large Ensemble Single Forcing Model Intercomparison Project (LESFMIP; Smith et al., 2022) to isolate the competing roles of ozone, GHGs and aerosols in driving multidecadal trends in the SH atmosphere and ocean. LESFMIP is a unique modelling intercomparison project because of: (a) the required large ensemble size, which allows for better quantification of internal variability; (b) the availability of multiple models, which allows for quantification of model uncertainty; and (c) the ability to isolate the roles of different forcings. In addition to revisiting simulated historical changes in SH circulation and their attribution to single forcings, as well as known model-observation discrepancies, we address several under-explored questions. These include seasonal variations in forcing attribution, the impact of aerosol forcing on observed SH changes, and the influence of ozone recovery on the SH climate post-2000.

2. Data and Methods

To explore the roles of different anthropogenic forcing agents, we use simulations from the LESFMIP database (Smith et al., 2022). These simulations followed the experiments proposed by the Detection and Attribution Model Intercomparison Project (DAMIP, Gillett et al., 2016) from Coupled Model Intercomparison Project Phase 6 (CMIP6, Eyring et al., 2016), but with increased ensemble size. LESFMIP simulations are a key component of the World Climate Research Programme Lighthouse Activity on Explaining and Predicting Earth System Change (EPESC, Findell et al., 2023) objective to establish and apply attribution methodologies to explain multi-annual to decadal changes in the climate system.

Four different types of LESFMIP experiments were considered: (a) *historical* experiment, forced by natural sources (observed volcanic aerosols, solar forcing, natural aerosols, etc.) and anthropogenic sources (observed GHG concentrations, ozone concentrations, anthropogenic aerosols and land use); (b) *hist-GHG* experiment, forced by varying GHG emissions as in the historical experiment while fixing the natural forcing and the other anthropogenic forcing at preindustrial values; (c) *hist-aer* experiment, forced by varying anthropogenic aerosol sources or concentrations as in the historical experiment while fixing the natural forcing and the other anthropogenic forcing at preindustrial values; and (d) *hist-totalO3* experiment, forced by varying total column ozone concentrations as in the historical experiment while keeping constant the natural forcing and the other anthropogenic forcings. This is notably different from the DAMIP stratospheric ozone only (*hist-stratO3*) experiment (Gillett et al., 2016), but is consistent with that proposed in DAMIP2 for CMIP7 (Gillett et al., 2025). Table 1 shows the number of members used for each model and experiment. All 10 models considered have conducted the historical, hist-GHG, and hist-aer experiments, but only 6 models included the hist-totalO3 experiment. Although the number of members varies according to the model and experiment, a minimum of 10 members for each set are available, while two thirds (24/36) of the simulations are run with larger ensemble sizes (20–65).

We use monthly outputs from LESFMIP simulations for the following variables: net top-of-atmosphere (TOA) radiative fluxes (based on downward solar, upward solar, and upward longwave radiative fluxes), mean sea level pressure (SLP), zonal and meridional wind (at all available pressure levels), SST, downward heat flux at sea water surface, sea water potential temperature (all vertical levels), sea ice area fraction, and precipitation. All the simulations were interpolated to a $2.5° \times 2.5°$ regular horizontal grid through bilinear interpolation or first-order conservative interpolation for globally defined fields. In each case, we use as many simulations as are available for each variable. For the analysis we consider monthly data and seasonal means for December–January–February

Table 1
LESFMIP Models, Experiments, and Number of Ensemble Members Used in the Study

Model	Experiments				Reference
	Historical	Hist-GHG	Hist-aer	Hist-totalO3	
ACCESS-ESM1-5	40	10	10	–	Ziehn et al. (2020), Mackallah et al. (2022)
CanESM5	65	50	30	10	Swart et al. (2019)
CMCC-CM2-SR5	10	10	10	–	Lovato et al. (2022)
CNRM-CM6-1	30	10	10	–	Voldoire et al. (2019)
GISS-E2-1-G	40	40	40	40	Kelley et al. (2020), Miller et al. (2021)
HadGEM3-GC31-LL	55	55	55	50	Jones et al. (2024)
IPSL-CM6A-LR	33	10	10	–	Boucher et al. (2020), Lurton et al. (2020)
MIROC6	50	50	10	10	Shiogama et al. (2023)
MPI-ESM1-2-LR	50	30	30	30	Mauritsen et al. (2019)
NorESM2-LM	43	23	23	20	Seland et al. (2020)

Note. See also Tables S1 and S2 in Supporting Information S1.

(DJF), March–April–May (MAM), June–July–August (JJA), and September–October–November (SON) or annual means.

In order to evaluate the long-term changes associated with the various forcings, we calculate the mean difference between the 35-year periods at the beginning (1850–1884) and the end (1980–2014) of the simulations. We also evaluate the temporal evolution for the full period (1850–2014 or 1850–2020 depending on the experiment and model) of different indices that describe some of the main features of the SH circulation and surface impact. To that end, we compute the multi-model mean (MMM) for each experiment, by first calculating the ensemble mean for each model and then averaging across all models with equal weights. We highlight grid points with 100% agreement in the sign of the ensemble mean response to indicate robustness of the response across models. As a caveat, 100% agreement among the model responses does not guarantee that the response is correct, as this could be related to a common model bias. We also acknowledge that the MMM can mask substantial differences in the responses across individual models. To better compare across individual models and to assess how each model compares to the true observed response, we also compute linear trends for the 1980–2014 period for the individual model runs with the aim of comparing them with observational results during the satellite era when more observations are available to constrain the reanalysis. Since the number of models varied across experiments, we tested whether selecting only those models for which simulations were available from all four experiments would affect the results. Finding no significant changes, we present the MMM results using all available models for each respective experiment.

The 1980–2014 analysis period mixes together the period of ozone depletion and ozone recovery, which have oppositely signed influences on the circulation. In order to evaluate the possible effect of ozone recovery in the beginning of the 21st century on the SH climate trends, and to more cleanly separate ozone depletion and recovery signals, in Section 3.5 we compare the linear trends for the 1980–1999 and 2000–2014 periods in both the models and the reanalyses. A caveat is that the models are forced with total column ozone changes, including changes in tropospheric ozone (Checa-Garcia et al., 2018), which precludes a clean attribution to stratospheric ozone depletion and recovery. Additionally, none of the LESFMIP models include interactive ozone chemistry, a model simplification which has been shown to result in a too-weak SH circulation response to ozone depletion (Haase et al., 2020; Ivanciu et al., 2021) and a weaker circulation response to ozone recovery that is more easily overcome by GHG forcing (Ivanciu et al., 2022).

We use the following observation-based data sets to compare with simulations: the fifth generation ECMWF atmospheric reanalysis (ERA5, Hersbach et al., 2020), the Modern-Era Retrospective analysis for Research and Applications, Version 2 (MERRA2, Gelaro et al., 2017), the Japanese 55-year Reanalysis (JRA-55, Kobayashi et al., 2015), the Japanese Reanalysis for Three Quarters of a Century (JRA-3Q, Kosaka et al., 2024), the Extended Reconstructed Sea Surface Temperature, Version 5 (ERSSTv5, Huang et al., 2017), the EUMETSAT

Ocean and Sea Ice Satellite Application Facility (OSI SAF, Lavergne et al., 2019), and the observational (station)-based SAM index (Marshall, 2003).

We define the Hadley cell edge as the latitude where the 500-hPa zonal-mean meridional mass stream function switches sign from negative in the SH tropics to positive in the SH mid-latitudes, and the eddy-driven jet latitude as the latitude where the 850-hPa zonal-mean zonal wind field is maximized at SH mid-latitudes. Both metrics are calculated using the Tropical-width Diagnostics code package (TropD; Adam et al., 2018), with the eddy-driven jet latitude found using the "max" method. Monthly mean wind fields are first zonally and then seasonally averaged prior to calculating the metrics. The SAM is defined as the difference in normalized monthly zonal mean SLP between 40°S and 65°S based on the Gong and Wang (1999) definition and using 1850–1884 for the standardization period. Final stratospheric warming (FSW) dates are estimated from monthly mean data following Hardiman et al. (2011), by assuming that the monthly mean data correspond to the 15th of each month and then creating a daily time series by linear interpolation. To find the day of the FSW we select the first day during austral spring on which the zonal mean zonal wind at 50 hPa and 60°S drops below 15 m s^{-1}. Sea ice concentration is defined as the percentage of each grid cell covered in sea ice, while sea ice extent is calculated as the total area of grid cells that have at least 15% sea ice cover. In Section 4, we consider the existence of a model-observation trend discrepancy using the 1980–2014 period if the following two criteria are met: (a) the observed trend (or the mean, if there is more than one estimate) falls outside the 5th and 95th percentiles of the distribution of all members, independently of the model; (b) for at least five models, the observed trend lies outside the full range of values in the distribution of all members.

3. Results

In this section, we assess long-term changes in the principal features of the SH climate and evaluate their potential attribution to anthropogenic drivers. Where applicable, we compare these changes with observations and evaluate their potential attribution to anthropogenic drivers. In particular, we evaluate the seasonal variations in the attribution of forcing, as well as the impact of aerosol forcing on the SH observed changes.

3.1. Radiative Fluxes at Top-of-Atmosphere (TOA) and Zonal-Mean Temperature Response

To understand how the radiative modifications resulting from the various forcing agents lead to changes in circulation and how these vary seasonally, we first explore changes in top-of-atmosphere (TOA) net downward all-sky radiative fluxes (Figure 1) and zonal-mean temperature (Figure 2) for 1980–2014 relative to the 1850–1884 reference period. The all-sky fluxes include cloud radiative effects and so may be more difficult to compare across models due to large differences in how models simulate cloud–aerosol interactions and other cloud-related processes. However, the all-sky fluxes also better represent the radiative forcing the dynamics respond to, and thus have a more meaningful connection to the rest of the analysis.

The historical simulations indicate increases in SH TOA energy fluxes (0.85 ± 0.25 W/m^2), with individual ensemble means ranging from 0.04 ± 0.12 W/m^2 (CMCC-CM2-SR5) to 1.21 ± 0.11 W/m^2 (ACCESS-ESM1-5). Both aerosols (0.49 ± 0.33 W/m^2) and GHGs (0.59 ± 0.22 W/m^2) make positive contributions in the hemispheric-mean TOA energy imbalance, though with different spatial distributions (Figures 1b and 1c). GHG increases lead to positive TOA energy fluxes that peak in the tropics and regions of maximum sea ice loss, whereas aerosols lead to positive flux changes over most SH ocean regions, with maxima in the subtropical anticyclone regions, and negative flux changes in most NH regions, especially in mid-latitude continental areas. It is interesting that both GHGs and aerosols lead to positive changes in net SH TOA radiative flux, despite GHGs leading to warming of global-mean surface temperatures and aerosols leading to cooling (Figure 2). This seeming contradiction can be explained by changes in cross-equatorial energy transport (e.g., Stephens et al., 2016); for example, the positive aerosol-related forcing in the SH implies increases in northward atmosphere/ocean energy exports to the NH under the hist-aer experiment. The response in SH TOA fluxes for hist-totalO3 (Figure 1d) is generally weaker than the responses for hist-aer or hist-GHG (Figures 1b and 1c). Ozone forcing averaged across the ensembles leads to predominantly negative TOA fluxes in the SH, particularly for Antarctica, consistent with reduced atmospheric absorption of solar radiation due to ozone loss that amplified in magnitude during the period of peak ozone depletion in the 1980 and 1990s before leveling off in the 2000s (Figure 1e).

Across model ensemble means, aerosol and GHG effects on the energy balance of the entire SH are of comparable magnitude in the annual mean (Figure 1e) but with distinctly different seasonalities that show considerable inter-

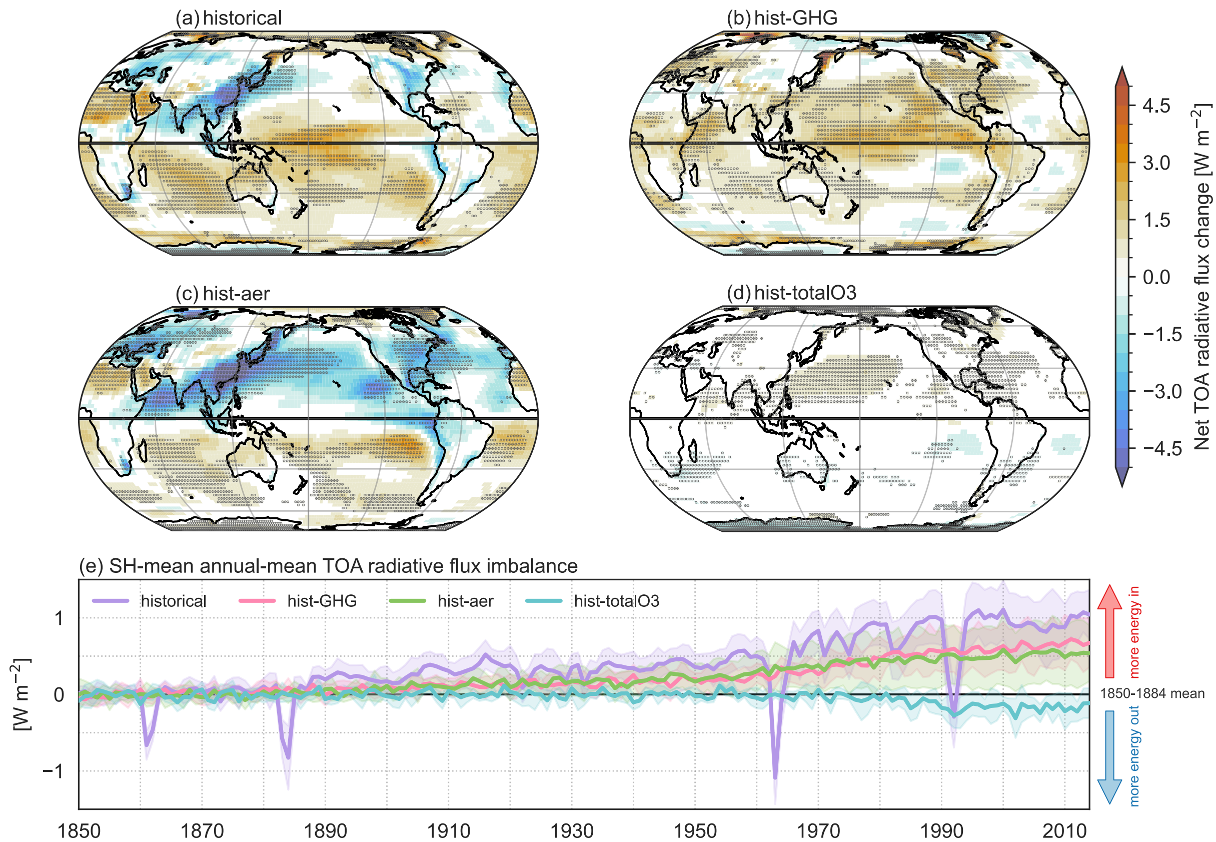

Figure 1. Changes in simulated net top-of-atmosphere (TOA) radiative fluxes for 1980–2014 relative to the 1850–1884 average (calculated across experiments but excluding historical to avoid pre-1884 volcanic influence). Spatial distributions based on (a) historical, (b) hist-GHG, (c) hist-aer, and (d) hist-totalO3 multi-model means. The stippling marks regions where all models agree on the response sign. (e) Time series of annual-mean TOA flux changes averaged over the entire Southern Hemisphere relative to the 1850–1884 period. The shading indicates ±1 standard deviation across model ensemble means. Units in W m^{-2}.

model differences. Inter-model spreads in all-sky TOA imbalance, clear-sky TOA imbalance, and cloud radiative effects are comparable in magnitude when plotted month-by-month (Figure S1 in Supporting Information S1). Cloud radiative effects contribute significantly to the DJF (summertime) spread in the all-sky TOA fluxes, especially under hist-GHG and hist-totalO3 (Figures S1i–S1l in Supporting Information S1). These inter-model differences are beyond the scope of this paper and will be evaluated in detail in follow-up work.

The zonal-mean temperature responses in Figure 2 include both radiative (Figure 1) and dynamically driven effects, most of which are well-known but with some interesting seasonal variations that we will point out here. The historical experiment shows year-round broad tropospheric warming that peaks in the tropical upper troposphere and stratospheric cooling that generally increases with altitude (Figures 2a–2d), responses consistent with the known response to GHG increases (Figures 2e–2h second column; see also Santer et al. (2023) and references therein). Year-round cooling of the polar lower stratosphere peaks in SON (austral spring) and DJF (Figures 2a and 2d), primarily from ozone forcing (Figures 2m and 2p; Thompson & Solomon, 2002). GHGs more weakly contribute to polar lower stratospheric cooling but with different seasonality than ozone, peaking in DJF and MAM (austral fall) (Figures 2e and 2f; Grise & Polvani, 2017). Ozone forcing in SON and DJF also produces a warming of the mid-stratosphere. This dipole polar temperature response to ozone depletion has been attributed primarily to enhanced shortwave cooling in the lower stratosphere and dynamical heating in the mid stratosphere (Keeble et al., 2014). Additionally, there is a year-round robust warming in the upper tropical troposphere and cooling in the tropical to subtropical lower stratosphere in response to ozone forcing. The hist-aer experiment shows broad tropospheric cooling that peaks in the upper tropical troposphere (Figures 2i–2l), which in the zonal-mean is spatially similar but opposite in sign to the GHG response. In contrast to GHGs which are well-mixed in the atmosphere, the influence of the more tropospherically confined anthropogenic aerosol forcing on stratospheric temperatures is generally weak for the long-term response; however, it is important to reiterate

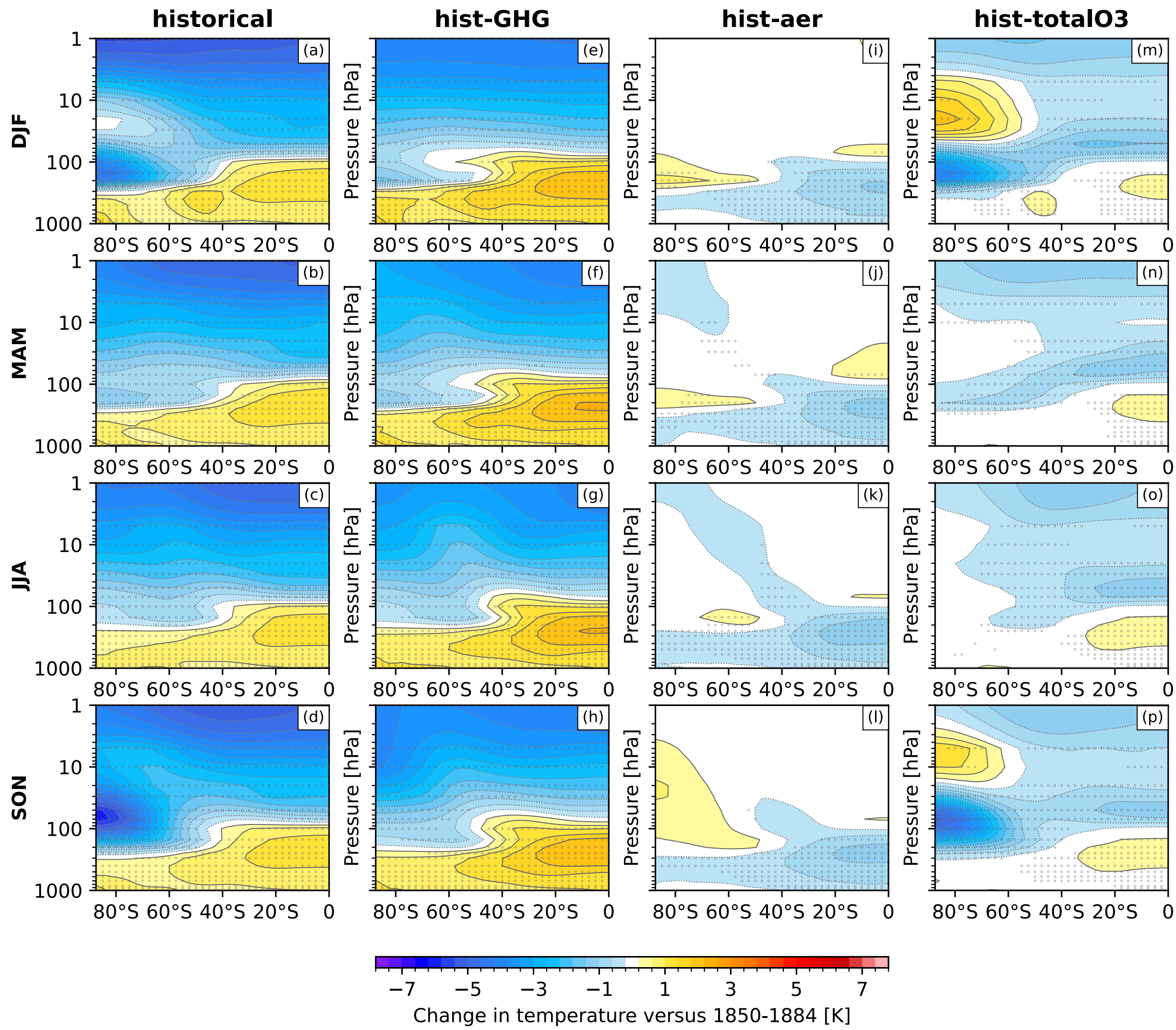

Figure 2. Zonal-mean temperature responses (difference between 1980–2014 and 1850–1884 periods, for multi-model ensemble mean) in shading starting from ±0.2°K for (top row) DJF, (second row) MAM, (third row) JJA, and (bottom row) SON, for the (a–d) historical forcings, (e–h) hist-GHG only, (i–l) hist-aer only, and (m–p) hist-totalO3 only. Units in K. The stippling indicates locations where all models agree on the sign of the response.

that the hist-aer simulation design excludes the significant short-term deviations that often occur following volcanic eruptions, when stratospheric aerosol loading is temporarily enhanced.

3.2. Large-Scale Atmospheric Circulation Responses

To address the large-scale changes in the SH atmospheric circulation, their seasonal variations and its potential attribution to single forcings, we show the zonal-mean zonal wind (Figure 3) and the SLP (Figure 4) responses for 1980–2014 relative to the 1850–1884 reference period in each season for the four LESFMIP experiments. The simulated historical zonal wind responses during SON and DJF have been well-documented (e.g., Eyring et al., 2013; Son et al., 2018): relative to the preindustrial climatology (black contours), the SON stratospheric polar vortex winds strengthen; the lower stratospheric westerly winds persist longer into DJF; while the tropospheric eddy-driven jet is enhanced on its poleward flank year-round, but with a distinct poleward shift in DJF (Figures 3a and 3d). In MAM, the models also agree on stronger zonal winds throughout the lower to mid stratosphere, with stronger winds on the poleward side of the tropospheric jet, but with a lower magnitude than DJF and SON, especially in the lower stratosphere. A broadly similar story is apparent in JJA, though in the stratosphere, the strongest increases occur on the equatorward flank of the polar vortex, and the tropospheric jet shows its strongest increases at its central jet location, in contrast to other seasons.

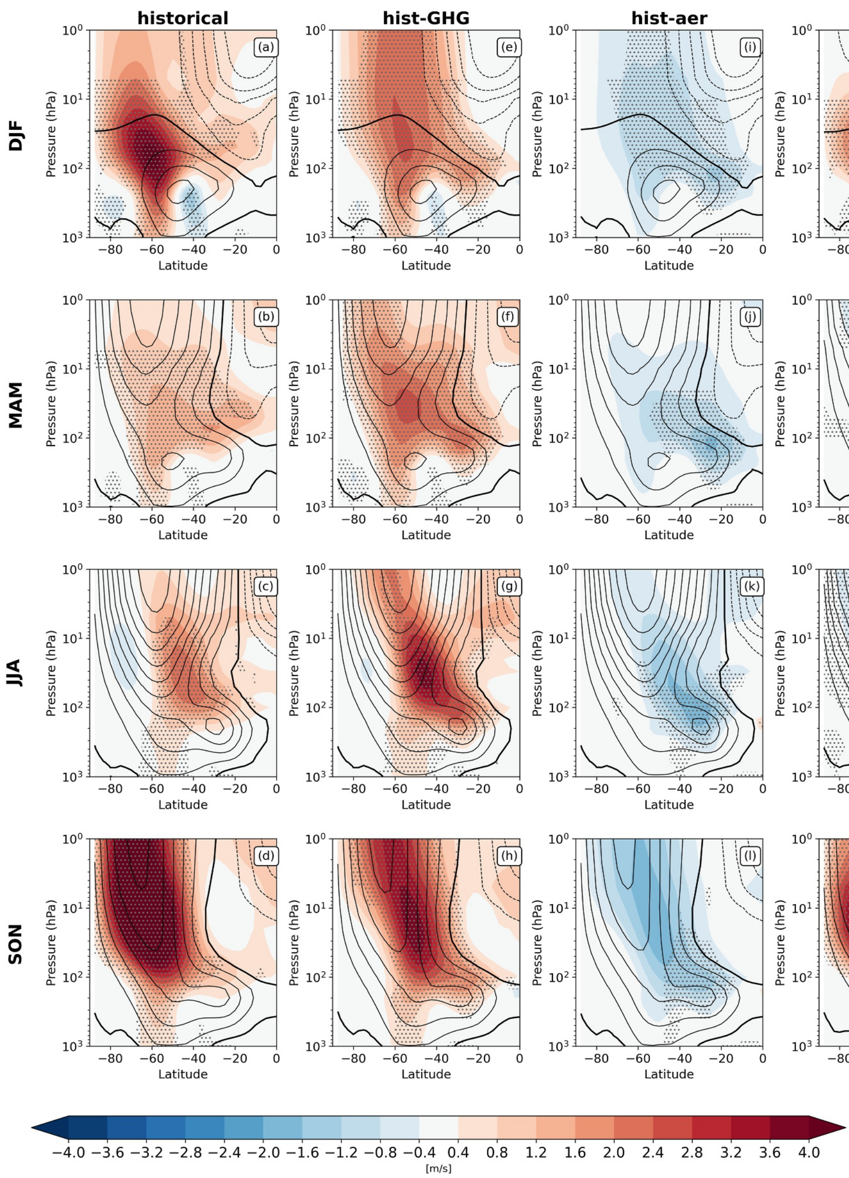

Figure 3. Zonal-mean zonal wind responses (difference between 1980—2014 and 1850–1884 periods, for multi-model ensemble mean) in shading for (top row) DJF, (second row) MAM, (third row) JJA, and (bottom row) SON, for the (a–d) historical forcings, (e–h) hist-GHG only, (i–l) hist-aer only, and (m–p) hist-totalO3 only. Units in m s^{-1}. The contours show the multi-model mean ensemble-mean climatology for the preindustrial period (1850–1884); the contour interval is 10 m s^{-1}, with the thick contour line representing 0 m s^{-1}. The stipping indicates regions where all models agree on the sign of the response.

In agreement with other studies, the magnitude of the SON and DJF zonal wind responses from the preindustrial era to the early 21st century appear to be about equally attributable to hist-GHG and hist-totalO3, though ozone forcing dominates in the last few decades of the simulations (not shown). Though both GHG and ozone forcings strengthen the westerly zonal winds in the extratropical stratosphere and contribute to a poleward shift of the tropospheric jet during the dynamically active seasons (SON and DJF), the structure of the zonal wind response is somewhat different between the two forcings. GHGs increase the polar stratospheric winds from the lower to upper stratosphere, particularly on the equatorward side of the climatological polar vortex in SON (Figures 3e–3h). On the other hand, ozone forcing primarily enhances the winds in the lower to mid stratosphere, with a stronger effect near or slightly poleward of the core of the climatological vortex winds (Figures 3m–3p). These differences likely reflect the different mechanisms by which each forcing affects the circulation. For

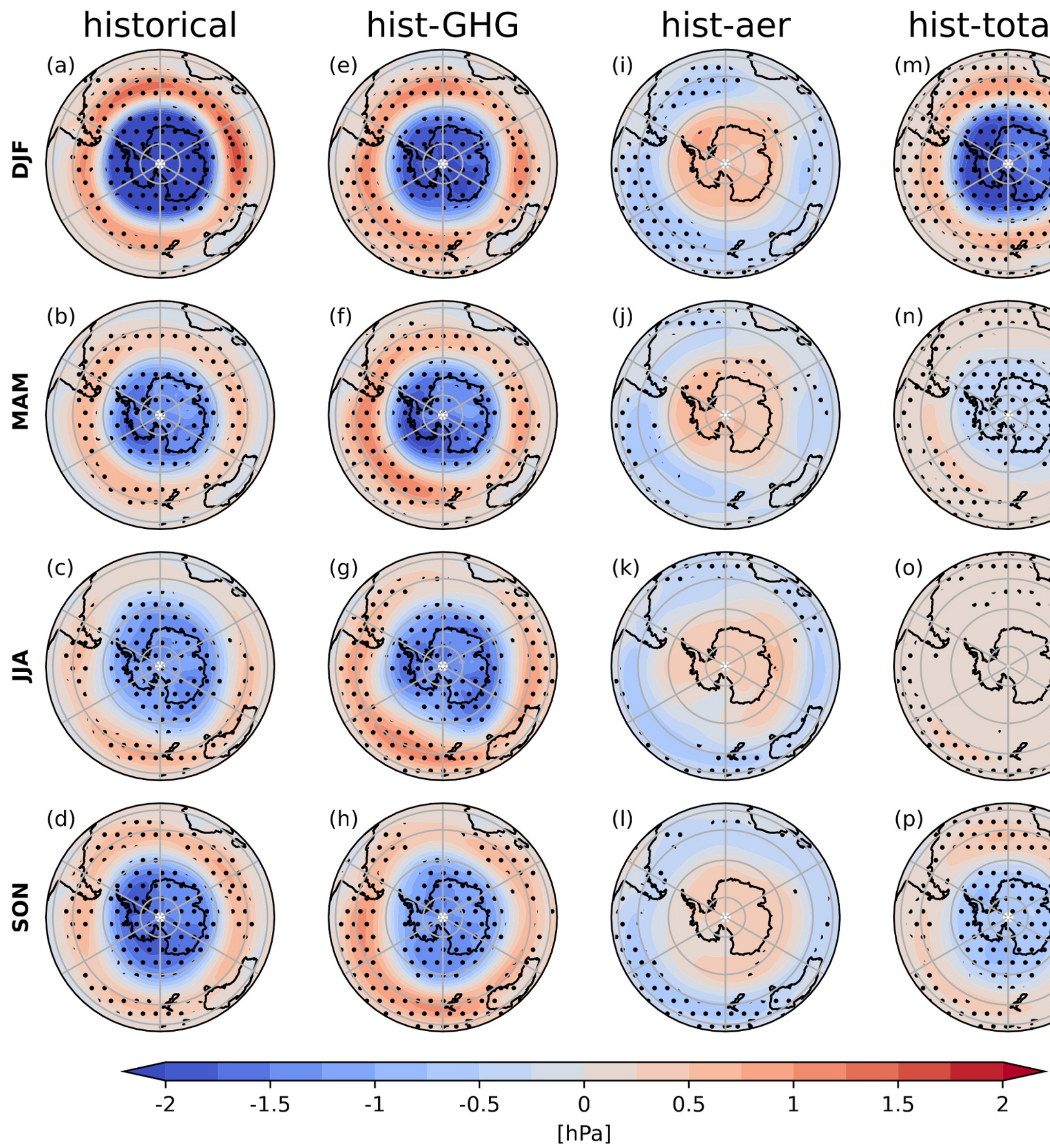

Figure 4. Multi-model mean sea level pressure response (difference between 1980–2014 and 1850–1884 periods) for (top row) DJF, (second row) MAM, (third row) JJA, and (bottom row) SON, for the (left column) historical, (second column) hist-GHG, (third column) hist-aer, and (right column) hist-totalO3 experiments. Units in hPa. The stippling indicates regions where all models agree on the response sign.

instance, ozone forcing acts primarily through positive chemical–dynamical feedbacks that drive a stronger and more persistent polar vortex in response to ozone depletion-driven cooling in the lower stratosphere (Figure 2). Conversely, GHG forcing predominantly enhances the zonal winds via thermal wind balance by sharpening the meridional temperature gradient across the subtropical tropopause (Wilcox et al., 2012), which occurs year-round (Figure 2). In both cases, changes in the temperature gradient near the tropopause (and for GHGs, at the surface) can also alter wave generation and propagation (McLandress et al., 2010). Interestingly, in JJA, ozone forcing instead decelerates the stratospheric polar vortex on its poleward flank (Figure 3o); however, this response is not robust in the historical simulations (Figure 3c). Aerosol forcing slows the lower to mid-stratospheric zonal winds in all seasons (Figures 3i–3l), with the most robust changes across models in the subtropical lower stratosphere (20–40°S). The zonal-mean zonal wind response to hist-aer tends to spatially mimic the response to hist-GHG (but is of the opposite sign, Figures 3e–3h), except that GHG forcing enhances the westerly winds more broadly from the lower to upper stratosphere and from the subtropics to the extratropics, whereas the only robust response to aerosol forcing occurs in the lower subtropical stratosphere. The stratospheric cooling under GHGs

(Figures 2e–2h) could amplify both the direct thermal wind response in the extratropics as well as the indirect, potentially non-linear response to changes in baroclinicity and wave driving (Walz et al., 2023), which may explain the differences in the zonal wind response compared to aerosol forcing that shows little long-term influence on stratospheric temperatures (Figures 2i–2l).

The zonal-mean circulation responses in Figure 3 correspond to surface (SLP) responses, shown in Figure 4. In the historical experiment, during DJF, MAM, and SON, and to a lesser extent during JJA, the models agree on the spatial pattern of the SLP response, with decreasing SLP across the southern high latitudes and pole, and increasing SLP across the SH mid-latitudes, indicating that the response projects strongly onto the positive phase of the SAM. This SLP response is consistent (via geostrophic balance) with the increase in the zonal-mean zonal winds around 60°S (Figure 3). The models show a large spread in the vicinity of the eddy-driven jet latitude (50°S approx).

To a large degree, the historical SLP response resembles the hist-GHG response (Figure 4). The hist-GHG response is larger in magnitude than the other single-forcing experiments in most seasons, with the exception of hist-totalO3 in DJF, and is opposite in sign relative to the hist-aer response. For hist-totalO3, as well as for the historical experiment, the response signal is largest during DJF. The agreement between models is high for the hist-GHG experiment across seasons, and for the hist-totalO3 experiment during DJF and SON, but is much less evident in the hist-aer experiment outside of the tropics/subtropics. These results are consistent with those reported by Gillett et al. (2013) for previous model generations and also include the transition seasons, which have distinguishable roles for individual forcings. For example, a robust high-latitude SLP response is seen even in MAM for the hist-totalO3 experiment.

Next, we explore the evolution of various indices that describe some of the main features of the SH large-scale atmospheric circulation: the Hadley cell edge latitude, SAM index, and FSW date. The computation of these indices is described in Section 2. Although previous studies have explored the forced responses to these metrics, mainly in DJF, here we quantify the seasonal differences in responses and the relative importance of ozone and aerosols compared to GHGs using a multi-model approach. We also show trends in the historical experiment for individual ensemble members over the 1980–2014 period; the large ensembles allow us to quantify where in the ensemble spread the reanalysis value lies, and thus determine the likelihood of a model-observation discrepancy.

Figure 5 (left column) shows the MMM evolution of the SH Hadley cell edge latitude from the four LESFMIP experiments. All individual model-means in the historical experiments show a poleward shift of the Hadley cell edge since the preindustrial era in all four seasons (not shown). This poleward shift is largest in DJF, when GHG and ozone forcings have comparable contributions. GHG forcing is the dominant forcing during all four seasons, with a secondary contribution from ozone forcing during SON and DJF. In most models, aerosol forcing contributes to an equatorward shift of the SH Hadley cell edge in JJA and SON, with the exception of NorESM2-LM (not shown). The MMM equatorward shift due to aerosols is one third to one half the magnitude of the response due to the GHG forcing in these seasons, and roughly the same magnitude due to the ozone forcing in SON. Note, however, that the total historical trend is only approximately 80% of the sum of the individual contributions (not shown), reflecting potential nonlinearity in the ozone and GHG forcing signals during DJF (see also Polvani et al., 2011). The conclusions here are generally consistent with those noted by previous studies using CMIP6 models (e.g., Grise & Davis, 2020), which were based upon fewer numbers of ensemble members.

To compare with the reanalysis, in Figure 5 (right column) we show linear trends in the Hadley cell edge over the 1980–2014 period for all ensemble members of each model in the historical experiment. The reanalyses show a poleward shift of the Hadley cell edge of 0.2–0.4° latitude per decade during all seasons except SON. In JJA and DJF, these reanalysis trends generally fall within the model ensemble spread, but exhibit greater poleward trends in SH Hadley cell extent than the MMM. In MAM (autumn), at least one reanalysis (ERA5) shows much larger poleward shifts compared to the MMM, and only one individual member (out of 414) has a poleward shift magnitude greater than ERA5. In SON, the reanalysis instead shows a small equatorward shift of the Hadley cell edge, which is in disagreement with the poleward shifts shown by every model-mean; however, approximately 20% of individual model members show an equatorward shift. As is apparent by the large scatter in the magnitude of the Hadley cell edge trends simulated by individual model members over the 1980–2014 period (Figure 5 right column), trends in individual members (or the single "realization" of the reanalysis) are dominated by internal variability, which can drive large Hadley cell edge trends over a 35-year period that can easily mask any forced circulation trend (Garfinkel et al., 2015; Grise et al., 2018). e.g., a decadal shift from the positive Interdecadal

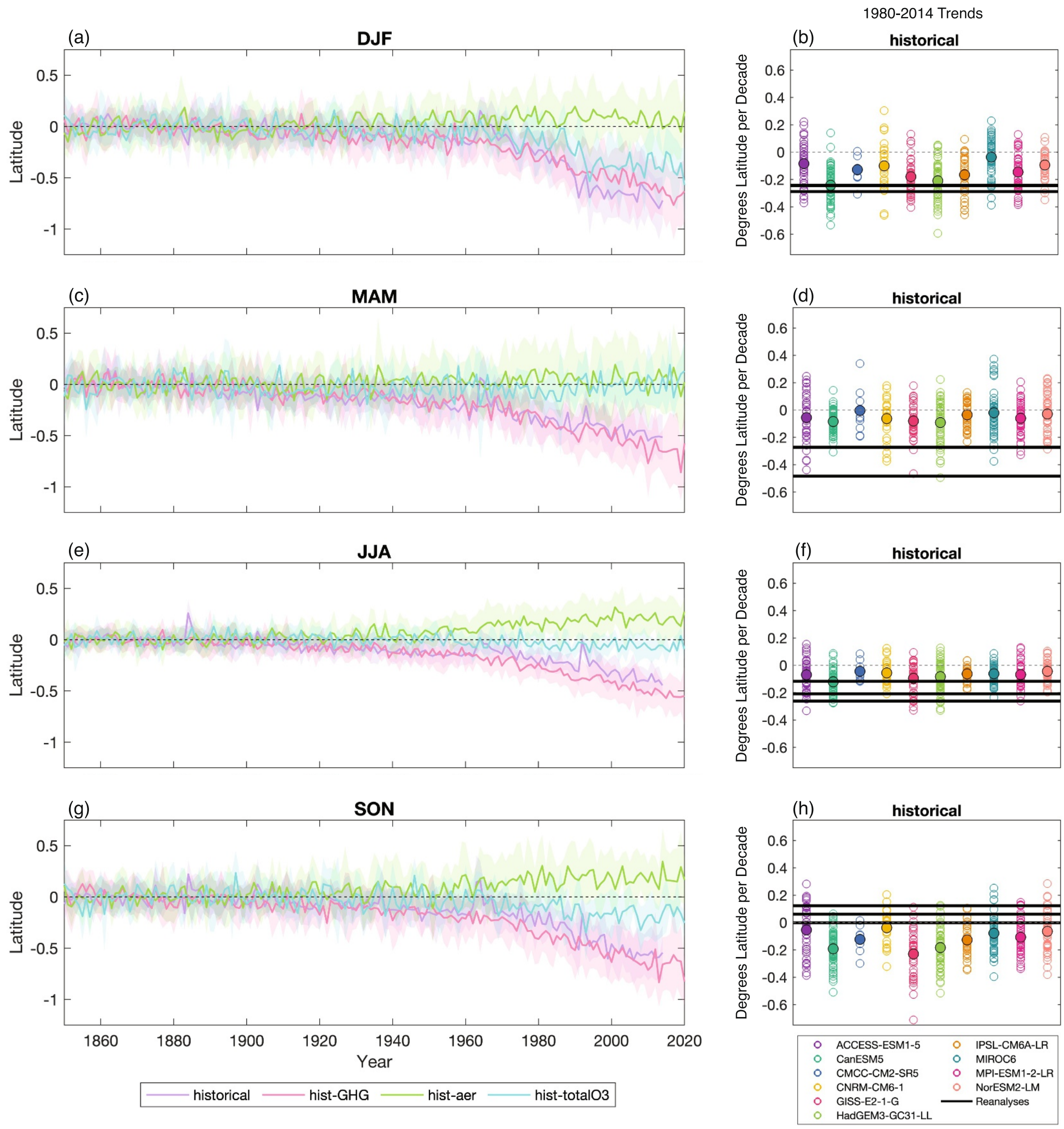

Figure 5. SH Hadley cell edge latitude year-to-year variabilities and long-term trends. Left column: Multi-model mean time series (1850–2020) of the four experiments (historical, hist-GHG, hist-aer and hist-totalO3) for each season: (a) DJF, (c) MAM, (e) JJA, and (g) SON. Values relative to 1850–1884 period. In each case, the shading indicates ±1 standard deviation across model ensemble means. Right column: Linear trends over 1980–2014 for historical experiment for each season: (b) DJF, (d) MAM, (f) JJA, and (h) SON. Open circles represent individual ensemble members, filled circles show model ensemble means, and horizontal lines indicate trends from ERA5, MERRA2, and JRA55 reanalyses.

Pacific Oscillation to its negative phase may be responsible for a significant portion of the observed Hadley cell expansion in recent decades (e.g., Allen & Kovilakam, 2017; Yang et al., 2020). Thus, the discrepancies noted above in MAM and SON between the reanalysis and models may arise from internal variability; or from a true model bias, given that the reanalysis value falls outside or at the far end of the ensemble spread for some models.

The behavior of the eddy-driven jet latitude (Figure S2 in Supporting Information S1) closely resembles that of the Hadley cell edge latitude (Figure 5), with a marked poleward shift, particularly during DJF. Two key differences between the Hadley cell edge and eddy-driven jet results are: (a) a greater role of ozone in driving the poleward shift of the eddy-driven jet during SON and DJF, and (b) a stronger role for aerosol forcing in counteracting the poleward shift of the eddy-driven jet position during DJF and MAM, but a weaker role during JJA and SON. Over the 1980–2014 period (Figure S2 in Supporting Information S1), a consistent poleward shift of the eddy-driven jet position is seen in DJF and MAM in the reanalyses; however, during JJA and SON, there are

10.1029/2025JD046229

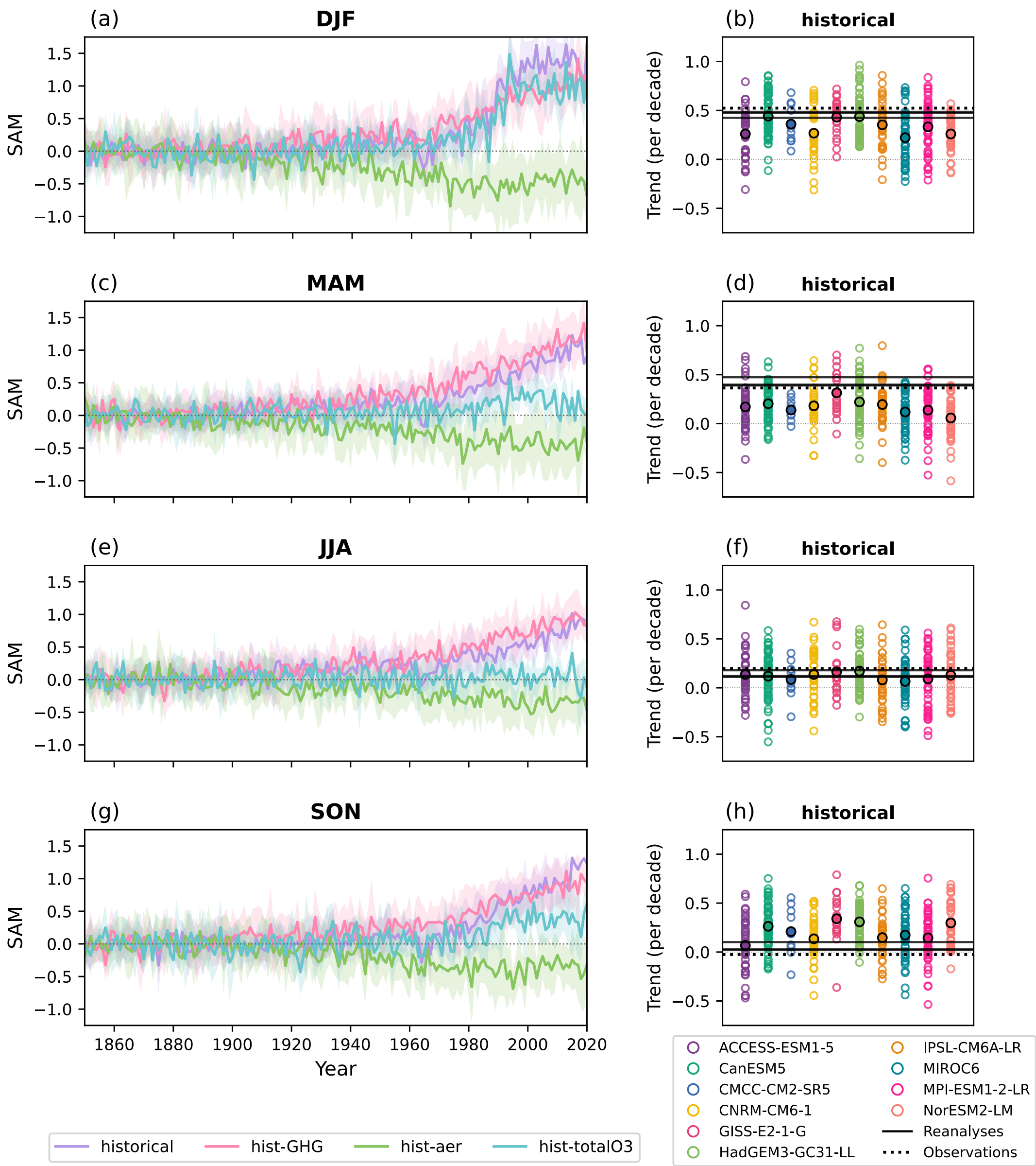

Figure 6. SAM index variabilities and trends. Left column: Multi-model mean time series (1850–2020) of the four experiments (historical, hist-GHG, hist-aer and hist-totalO3) for each season: (a) DJF, (c) MAM, (e) JJA, and (g) SON. The SAM is defined as the difference in normalized monthly zonal mean SLP between 40°S and 65°S based on the Gong and Wang (1999) definition and using 1850–1884 as the standardization period. In each case, the shading indicates ±1 standard deviation across model ensemble means. Right column: Linear trends over 1980–2014 for historical experiment for each season: (b) DJF, (d) MAM, (f) JJA, and (h) SON. Open circles represent individual ensemble members, filled circles show model ensemble means, and horizontal black lines indicate trends from ERA5, MERRA2, and JRA55 reanalyses (solid lines) and from station-based observations (Marshall, 2003, dotted lines).

instead near-zero or equatorward trends in the reanalyses. The model-means closely match these trends in DJF and JJA; but show a weaker poleward trend than reanalysis in MAM and near-zero or poleward trends in SON. However, the reanalysis trends still fall within the ensemble spread. The conclusions are generally consistent with those noted by previous studies using CMIP6 models (e.g., Lachmy, 2022; Mindlin et al., 2025), which were based upon fewer numbers of ensemble members.

Figure 6 shows clear positive trends for the MMM SAM index in the historical experiment, which accelerated around 1960 and are evident across all seasons but particularly pronounced during DJF and weaker in winter (JJA)

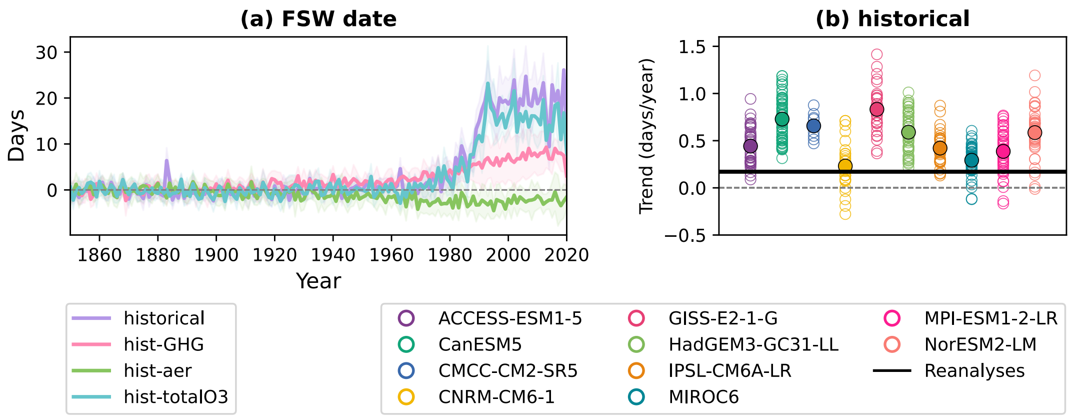

Figure 7. Final stratospheric warming (FSW) date variabilities and trends. (a) Multi-model mean time series (1850–2020) of the four experiments (historical, hist-GHG, hist-aer and hist-totalO3). Values relative to the 1850–1884 period. In each case, the shading indicates ±1 standard deviation across model ensemble means. (b) Linear trends over 1980–2013* for historical experiment. Open circles represent individual ensemble members, filled circles show model ensemble means, and solid black lines indicate trends from ERA5, MERRA2, and JRA-3Q reanalyses. *The FSW date can fall between October to the following January. This means that for several simulations we could not define the FSW date for 2014 because the record ended in Dec 2013. For this reason we only look at trends from 1980 to 2013 for this metric. The year 2002 was excluded from the computation of the FSW reanalyses trends because a sudden stratospheric warming occurred.

compared to the other seasons. This behavior is consistent with the poleward shift in the SH eddy-driven jet (Figure S2 in Supporting Information S1), SH Hadley cell edge (Figure 5) and the positive SAM-like pattern observed in mean SLP (Figure 4).

The single-forcing experiments reveal distinct seasonal patterns that help attribute the historical SAM trends (Figure 6). The hist-GHG experiments show consistent positive trends (in the MMM) across all seasons, reflecting the year-round influence of GHG forcing on the mid-latitude circulation (e.g., Arblaster et al., 2011; Shaw et al., 2024). In contrast, the hist-totalO3 experiments show marked seasonality, contributing equally with GHG during DJF when the impacts of the stratospheric ozone depletion on the troposphere are greatest; to about half of the positive trends in SON when Antarctic ozone depletion occurs (e.g., Thompson et al., 2011); and with weak or near-zero contributions during MAM and JJA, respectively (e.g., Purich et al., 2026). The hist-aer trends instead show surprisingly robust negative trends in the SAM, especially in DJF and SON. A negative SAM response to hist-aer is also seen in MAM and JJA, though the model spread is large and spans zero. Particularly for DJF, this model intercomparison suggests that the positive SAM trend in DJF due in equal parts to GHG and ozone would have been much larger without the mediating influence of aerosol forcing.

Over 1980–2014, the reanalyses, observations, and models agree on strong positive SAM trends during DJF (Figure 6b) (e.g., Fogt & Marshall, 2020), with much weaker positive trends in JJA (Figure 6d) and SON (Figure 6h). In MAM (Figure 6f), the reanalysis/observations show stronger positive trends relative to most individual model-means, but still lie within the ensemble spread for all models except CMCC-CM2-SR5 and NorESM2-LM. The substantial scatter among individual model members, with ranges frequently spanning zero, reflects the influence of internal variability over this shorter time period. This enhanced MAM trend in the reanalyses is consistent with the Hadley cell edge (Figure 5) and eddy-driven jet (Figure S2 in Supporting Information S1) shifts discussed above, indicating that three different circulation metrics all show larger poleward trends in observations than in the model ensemble mean during this season.

The FSW date time series are shown in Figure 7a. In the historical experiment, the MMM FSW occurrence is delayed by about 20 days between 1960 and the early 1990s, a large part of which can be explained by ozone depletion (e.g., Byrne & Shepherd, 2018). This attribution of the FSW delay using 6–10 different climate models supports the findings from McLandress et al. (2010), who used single forcing experiments of a single climate model. The FSW trend flattens out after the 1990s and even shows some indication of starting to reverse due to ozone recovery (see Section 3.5). Another factor contributing to the delay in FSWs in recent decades is the increase in GHGs, while aerosol forcing counteracts this positive trend slightly. Our results also suggest that increased GHGs may have contributed to later FSWs relative to the preindustrial period since even the early

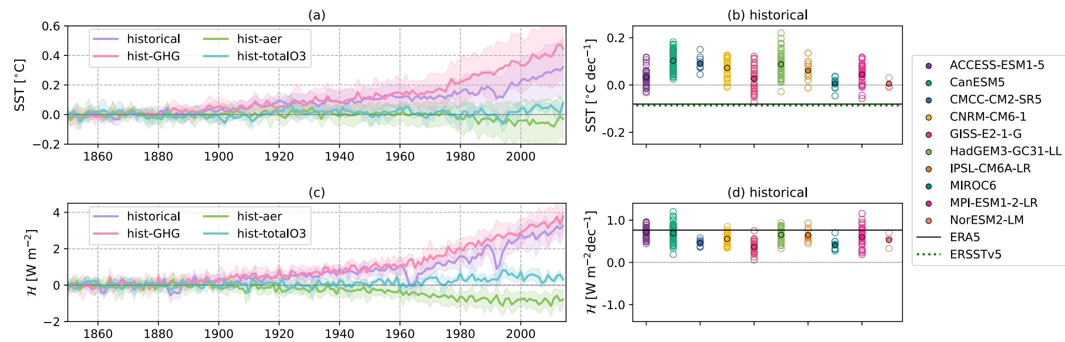

Figure 8. (a) Multi-model mean time series of spatially averaged (poleward of 50°S) annual-mean sea surface temperature (SST) of the four experiments (historical, hist-GHG, hist-aer and hist-totalO3). Units in °C. Values relative to the 1850–1884 period. In each case, the shading indicates ±1 standard deviation across model ensemble means; (b) SST linear trends over 1980–2014 for historical experiment. Open circles represent individual ensemble members, filled circles show model ensemble means, and the horizontal black lines are the observational trends from ERA5 (solid line) and ERSSTv5 (dashed line). Units are in °C/decade. Panels (c, d) Same as panels (a, b), but for the air-sea heat flux (H, positive values indicate flux into the ocean). Units are in Wm^{-2} and Wm^{-2}/decade respectively. Note that ocean diagnostics for many ensemble members for a number of models are not available, so only those ensemble members that had all three diagnostics– SSTs, air-sea heat flux and ocean temperatures– were analyzed. For details, see Text S1 and Table S1 in Supporting Information S1.

1900s, with a larger role than ozone forcing until the 1970s. Surprisingly, aerosol forcing has counteracted this influence, leading to earlier FSWs; while this opposing influence has not grown in magnitude since 1960, these simulations indicate that it has clearly mediated the later timing of the FSW due to GHGs and ozone for several decades now.

These findings are supported when considering the model trends for the shorter period of 1980–2013 (Figure 7b, Figure S3 in Supporting Information S1). All models agree on a delay of FSW in the historical experiment (Figure 7b), although the spread among individual model members can be very large, with some members even producing a negative trend (see e.g. the CNRM-CM6-1 model). The individual model mean trends range from ~0.23 days/year to ~0.83 days/year, which is larger than the trend estimated from reanalysis products during this period (~0.17 days/year). In fact, for 4 out of 10 models, the reanalysis value lies completely outside the model spread, though the reanalysis FSW trend is very sensitive to the start- and end-year of the period chosen.

3.3. Southern Ocean Response

We next explore the trends in the Southern Ocean temperatures (Figures 8–10) and Antarctic sea ice concentrations (Figure 11), including some model-observation discrepancies reported previously. Figure 8 shows the changes of annual-mean MMM SST and air-sea heat flux anomalies in the Southern Ocean for LESFMIP simulations. Note that we analyze spatial means over ocean regions south of 50°S; using slightly different latitude ranges did not change our conclusions qualitatively.

There is general agreement across the models of a long-term increase in Southern Ocean SSTs and heat uptake (positive heat flux) in the historical simulations (Figures 8a and 8c). This increase in SSTs and heat uptake is mostly driven by GHG forcing, while hist-aer simulations show a weak decline in SSTs but more robust negative heat flux that partially offsets the effects of GHG forcing. Of particular note, while trends towards a positive SAM and enhanced high-latitude surface westerlies–driven equally by GHG and ozone forcing in DJF (Figure 6)–should drive northward Ekman transport and SST cooling, the hist-totalO3 experiment shows instead negligible SST warming and a weakly positive heat flux into the ocean since ~1960 for annual-mean as well as DJF (not shown), in agreement with previous studies (e.g., Bitz & Polvani, 2012; Dong et al., 2023; Seviour et al., 2019; Sigmond & Fyfe, 2010).

Despite the models consistently showing warming of the Southern Ocean over the 1980–2014 period (Figure 8b), the ERA5 reanalysis and ERSSTv5 observations instead show a significant negative trend in Southern Ocean SSTs (approximately −0.09°C per decade). This is a common discrepancy among coupled climate models (e.g., Wills et al., 2022). Though there is a noticeable spread across models, with some models (MIROC6, NorESM2-LM, GISS-E2-1-G) showing much weaker positive trends than other models, only one model (GISS-

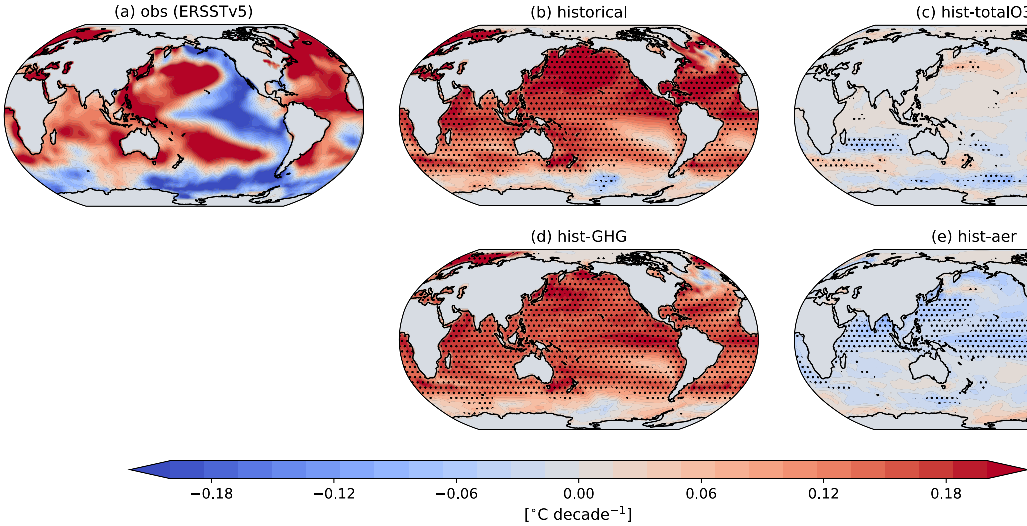

Figure 9. Multi-model mean DJF sea surface temperature (SST) trends from 1980 to 2014 for (a) ERSSTv5 (b) historical, (c) hist-totalO3, (d) hist-GHG, and (e) hist-aer experiments. Units in °C per decade. The stippling indicates regions where all models agree on the sign. The included models are those for which simulations were available from all experiments (CanESM5, GISS-E2-1-G, HadGEM3-GC31-LL, MIROC6, MPI-ESM1-2-LR and NorESM2-LM), and the number of ensemble members listed in Table 1 was used.

E2-1-G) has one member that shows trends equivalent to reanalyses and observations. Because these models generally simulate realistic SAM trends over this period (Figure 6), and interannual SAM-SST relationships are generally well-captured in CMIP models (e.g., Dong et al., 2023), poor simulation of the SAM seems unlikely to be the source of this discrepancy with observations, though it is possible models cannot capture SAM-SST relationships on multi-decadal timescales. Other proposed sources of the model-observation discrepancy in Southern Ocean SST trends are biases in radiative fluxes due to weak stratocumulus cloud feedback in coupled climate models (Kang et al., 2023); biases in ocean stratification and heat transport due to coarse resolution (Kang et al., 2026; Yeager et al., 2023); and missing freshwater fluxes from melting ice shelves (Kaufman et al., 2025; Schmidt et al., 2023). Further investigation is needed to identify the exact cause of this discrepancy between models and observations. In contrast, for trends in annual-mean heat flux into the Southern Ocean over the 1980–2014 period, positive trends in the ERA5 reanalysis are consistent with those simulated by the models (Figure 8d). There is also relatively more agreement and smaller spread among models for the heat flux trends compared to SST trends. However, the model-means underestimate the magnitude of the ERA5 trend, though many individual ensemble members show comparable magnitudes.

An examination of maps of SST responses in DJF better elucidates where the model-observation discrepancies are largest (Figure 9). While the observations show broad cooling across the Southern Ocean, the magnitude of the cooling trends is greatest in the Pacific sector (Figure 9a). Furthermore, a well-known "La Niña-like" cooling pattern is seen in the tropical Pacific (Jiang et al., 2024; Watanabe et al., 2024). In contrast, the historical simulations show weak SST warming of the Southern Ocean and much stronger magnitude SST warming over much of the rest of the globe (Figure 9b). Global SST warming is attributable primarily to GHGs (Figure 9d). Note that while some studies have suggested aerosols as the primary driver of the observed La Niña-like SST trend pattern (Hwang et al., 2024), here we instead see broad SST cooling of the tropics and subtropics but no significant meridional Pacific SST gradient due to aerosols (Figure 9e). Dong et al. (2025) suggested that stratospheric ozone changes have contributed to the observed tropical La Niña-like SST trend patterns based on a single model. In addition, we found a strong La Niña-like SST trend pattern associated with the ozone depletion period (1980–1999) that is obscured in the full period by small magnitude trends with low agreement between models during the ozone recovery period (2000–2014) (Figure S4 in Supporting Information S1). Therefore, the ozone forcing response is sensitive to the chosen time period. Our results provide some evidence that ozone forcing leads to cooling SST trends in the subtropical eastern Pacific and the Pacific sector of the Southern Ocean during DJF (though these responses are likely muted in the hist-totalO3 experiments due to a warming contribution from tropospheric ozone trends; Sigmond & Polvani, 2026). These results highlight the need to further investigate the

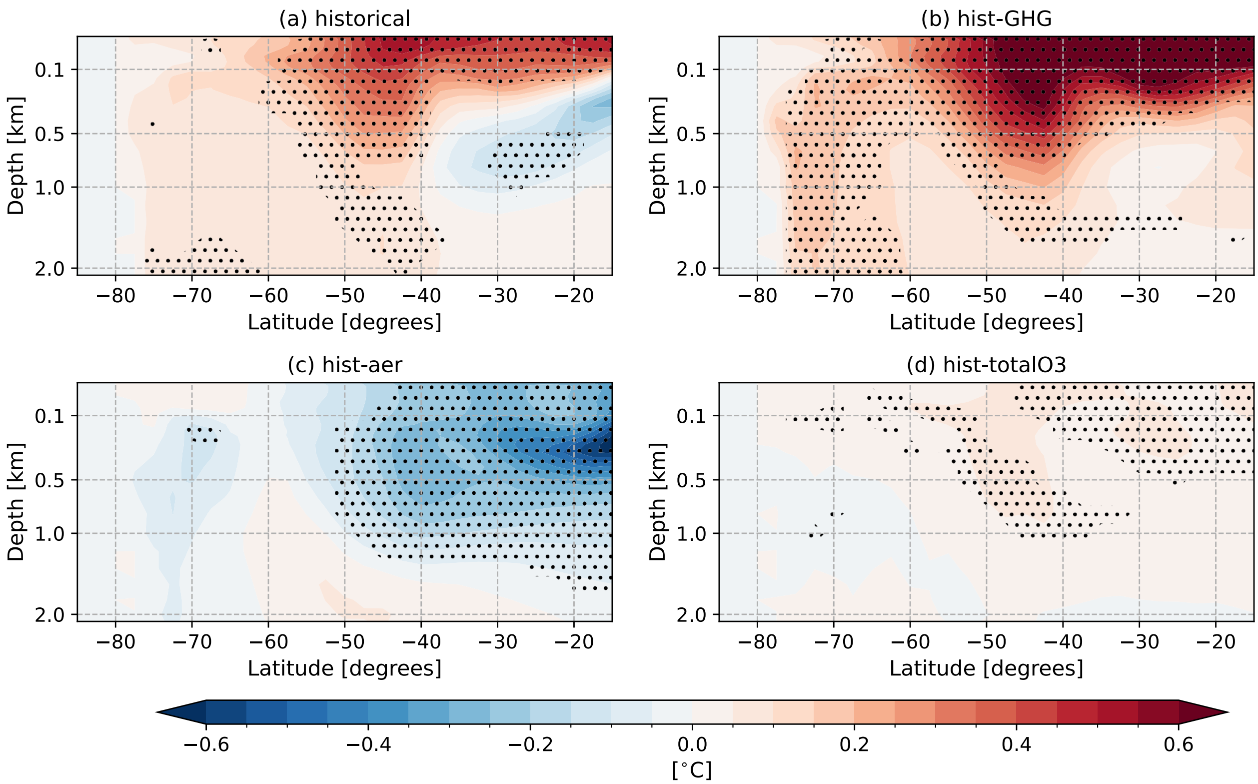

Figure 10. Multi-model mean zonal-mean ocean temperature response (difference between 1980–2014 and 1850–1884 periods) for (a) historical, (b) hist-GHG, (c) hist-aer, and (d) hist-totalO3 experiments. Units are in °C. The stippling indicates regions where all models agree on the response sign. Note that ocean diagnostics for many ensemble members for a number of models are not available, so only those ensemble members that had all three diagnostics –SSTs, air-sea heat flux and ocean temperatures– were analyzed. For details, see Text S1 and Table S1 in Supporting Information S1.

impact of stratospheric ozone trends on SH SST trends, and the potential role they play in model-observation discrepancies.

We now examine the long-term SH sub-surface ocean temperature response, along with the associated depth–latitude pattern of zonal-mean temperature anomalies (Figures 10a–10d). In historical simulations (Figure 10a), the warming extends as deep as 2 km at latitudes south of 40°S, which could be related to the Antarctic Intermediate Water that subducts the heat from the Southern Ocean below the subtropical water near the surface. Despite discrepancies between observations and models regarding Southern Ocean SSTs, the depth–latitude pattern of zonal-mean temperature changes resembles reported changes in the IAP/CAS ocean reanalysis over the 1940–2021 period (Cai et al., 2023). This warming is predominantly driven by the increase in GHGs (Figure 10b). In contrast, aerosol forcing leads to a net cooling, partially offsetting the warming caused by GHGs (Figure 10c). The cooling effect due to aerosols is mainly concentrated at latitudes north of 50°S and there is little signal at 70°S consistent among all models. In contrast, ozone forcing is associated with a weak warming trend, particularly in the upper 1 km and at latitudes north of 50°S (Figure 10d). These results confirm previous findings that GHGs and aerosols are the main drivers of Southern Ocean temperature changes below the surface (Chen et al., 2022), with ozone forcing playing a smaller role (Swart et al., 2018).

Figure 11 shows the evolution of MMM Antarctic sea ice extent (SIE) anomalies across the 1850–2014 period for each of the four LESFMIP experiments for both the sea ice minimum in February (Figure 11a) and the sea ice maximum in September (Figure 11c). Note that MIROC6 is not included in the sea ice analysis because it had very poor representation of Antarctic sea ice as reported in previous studies (e.g., Casagrande et al., 2023). For the historical simulation, the MMM shows a decline in SIE across the period for both months, with amplified negative anomalies occurring after ∼1960 (Figures 11a and 11c). The simulated reduction in SIE is physically consistent with the simulated increase in Southern Ocean temperatures (Figures 8 and 10). The SIE trends in the hist-GHG experiment are consistent with those based on the historical experiment, including larger inter-model spread

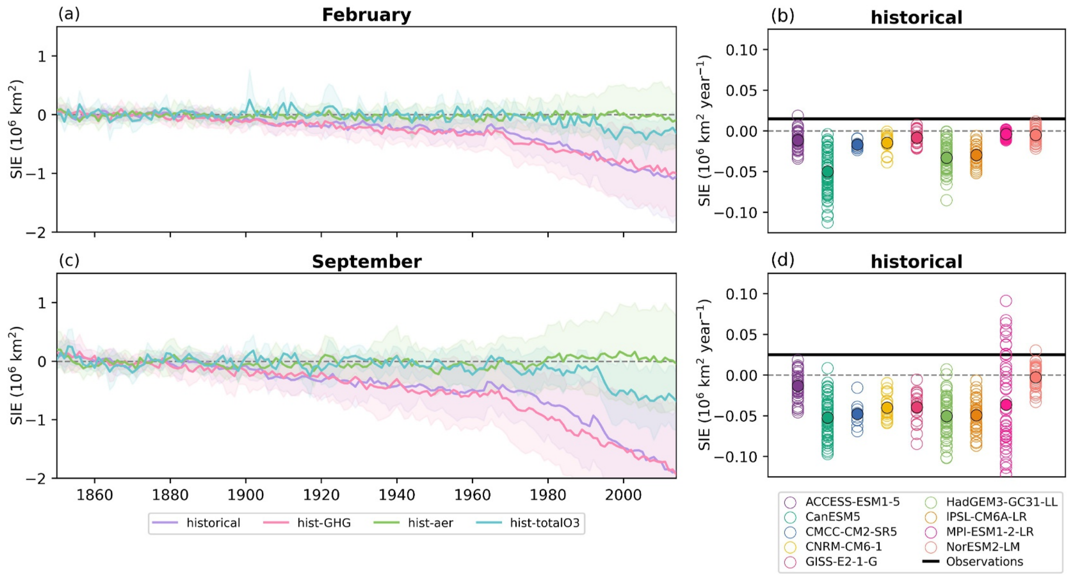

Figure 11. Sea ice extent (SIE) variabilities and trends. Left column: Multi-model mean time series (1850–2014) of the four experiments (historical, hist-GHG, hist-aer and hist-totalO3) for (a) February and (c) September. Values relative to the 1850–1884 period. In each case, the shading indicates ±1 standard deviation across model ensemble means. Right column: Linear trends over 1980–2014 for historical experiment for (b) February and (d) September. Open circles represent individual ensemble members, filled circles show model ensemble means, and horizontal black line is the observational trend from OSI-SAF (solid line). Note that sea ice variables for some ensemble members for a number of models were not available. For details, see Text S1 and Table S2 in Supporting Information S1.

during September. The spread across models is even larger in the hist-aer experiment, resulting in a neutral trend in the MMM. Finally, the SIE trend in the ozone forcing experiment is generally negative across the models over this time period. The small contribution from ozone forcing nonetheless shows a clear seasonality, with a larger impact on SIE anomalies during September compared to February, which is consistent with the seasonality of SIE response to stratospheric ozone depletion reported in Sigmond and Fyfe (2010). Figure S5 in Supporting Information S1 shows maps of the MMM Antarctic sea ice concentration (SIC) long-term response for each experiment and season. These maps indicate a widespread, year-round decrease in SIC in the historical experiment, primarily due to GHG forcing. Conversely, SIC changes in the hist-aer experiment are weaker and more heterogeneous across space, with greater disagreement among the models. Changes in SIC in the ozone forcing experiment are weakly negative, with smaller areas of 100% agreement among the models (Figure S5 in Supporting Information S1).

On balance, these results indicate that the modelled negative SIE trend from the historical simulation can be explained primarily by GHG forcing, with a small contribution from ozone forcing. These results are consistent with those of Sigmond and Fyfe (2014), who identified GHG forcing as the dominant driver of the simulated historical sea ice trend. Also consistent with our results, climate models show decreases in Antarctic sea ice in response to ozone depletion (Bitz & Polvani, 2012; Sigmond & Fyfe, 2010, 2014), as the increased westerlies act to enhance upward transport of relatively warm water over long timescales (Ferreira et al., 2015; Holland et al., 2017; Seviour et al., 2019).

While the models are generally consistent with each other, the observed evolution of sea ice extent over the more recent historical period is notably different from the simulated evolution of SIE, experiencing a slight positive trend from 1979 to 2015, followed by a rapid decline from 2016 to present day (e.g., Suryawanshi et al., 2023). This apparent model-observation discrepancy of sea ice trends is also captured in the second column of Figure 11, which shows individual models' ensemble member trends in SIE over the 1980–2014 period. Most ensemble members across all models are unable to capture the observed positive trend (black solid line), instead simulating a negative trend consistent with the long-term evolution (Figures 11a and 11c), particularly in February. The SIE trends model-observation discrepancy could be connected to the Southern Ocean SST trend discrepancy, as they may have a common origin (e.g., Schneider & Deser, 2018). There is a larger spread in the September SIE trends

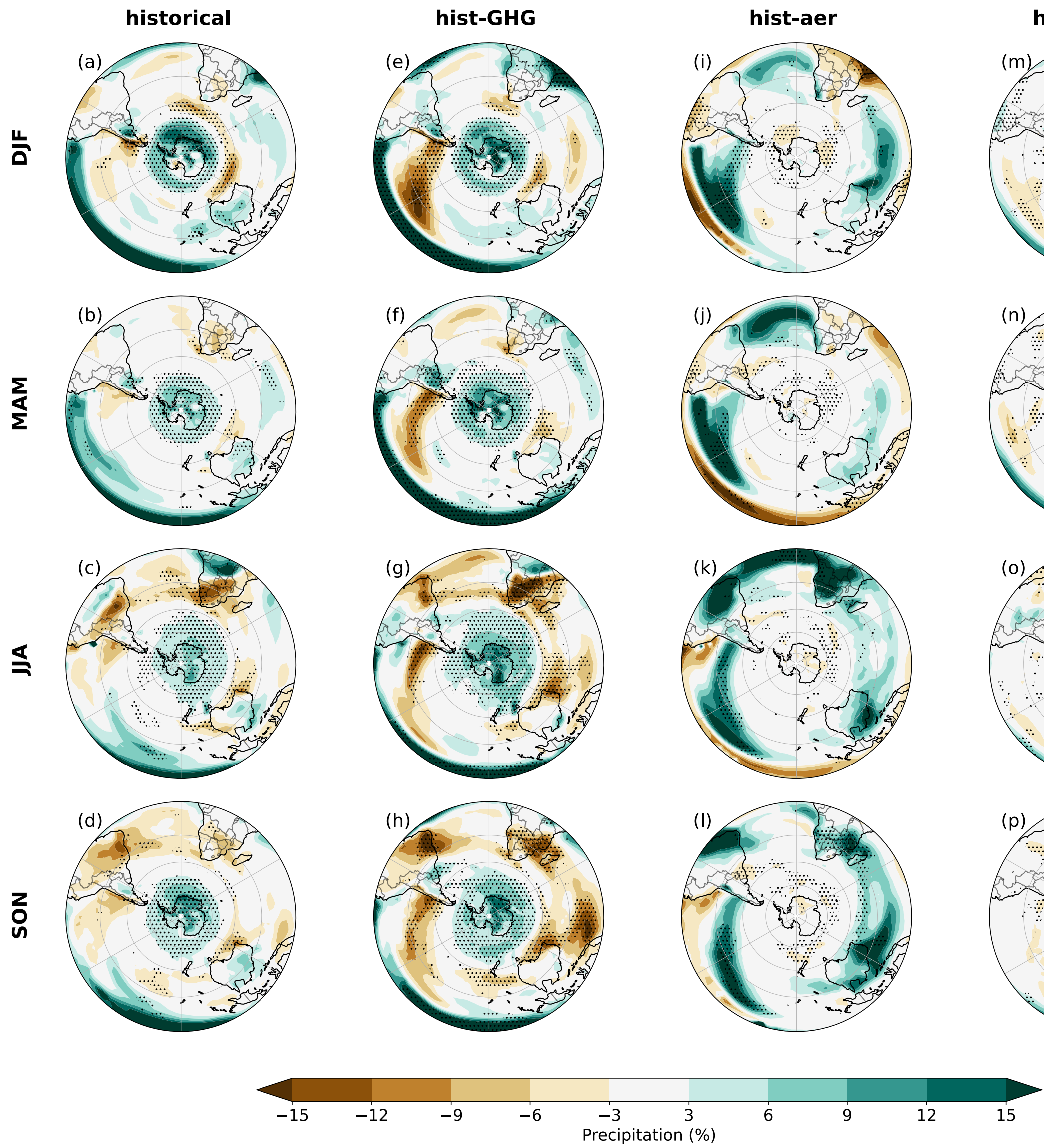

Figure 12. Multi-model mean percentual precipitation response (difference between 1980–2014 and 1850–1884 periods) for (top row) DJF, (second row) MAM, (third row) JJA, and (bottom row) SON, for the (left column) historical, (second column) hist-GHG, (third column) hist-aer, and (right column) hist-totalO3 experiments. The stippling indicates regions where all models agree on the response sign.

compared to the February SIE trends which is likely due to the seasonal cycle of SIE; a climatologically larger sea ice pack could result in more regional variability amongst the members. However, it is worth noting that a few members simulate a positive trend in the historical experiment (consistent with, e.g., Roach et al., 2020; Holmes et al., 2024), indicating that the observed trend falls within the possible range of simulated internal variability. The rapid decline in Antarctic sea ice since 2016 (not included in Figure 11) has brought broader alignment between observations and models for trends up to 2023 (Holmes et al., 2024). Additional large ensemble comparisons including the recent decade will be critical for further examination of the SIE model-observation discrepancy.

3.4. Precipitation Response

Next, we evaluate the impact of the anthropogenic forcings on precipitation and their seasonal differences (Figure 12). All models show a robust increase in high latitude precipitation throughout the year, surrounded by a decrease in the subtropics and mid-latitudes, with large regional and seasonal variability (Figures 12a–12d). The subtropical drying band is related to the poleward shift of the Southern Hadley cell edge (Figure 5). Furthermore, it exhibits zonal asymmetries, with many centers of action located over the oceans, as indicated by Schmidt and Grise (2017). On the other hand, the mid-latitude drying/high latitude wettening trend is consistent with the SAM positive trend (Figure 6), which drives a poleward shift of the SH storm tracks. The mid-latitude drying band, with high agreement between models, is only clearly evident in DJF when the eddy-driven jet is zonally symmetric, coincident with more negative trends in the low level extratropical zonal winds during this season (Figure 3a). This feature could be connected to the observed drying trend in southwestern South America (Boisier et al., 2018). In the other seasons, the primary drying band is located in the subtropics in the MMM, but with little agreement across the ensembles for most regions. Although there are almost no continental areas in the mid-latitudes where all models agree on the sign of change, eastern Australia and southeastern South America stand out for positive precipitation trends in DJF (e.g., Bandoro et al., 2014; Hendon et al., 2007; Kang et al., 2011), the latter region of which is well supported by analysis of observations since the beginning of the 20th century (e.g., Díaz et al., 2021).

Simulated SH rainfall changes in the historical experiment are mostly explained by GHG forcing with the exception of the tropical and southeast Pacific (Figures 12e–12h). While the hist-GHG experiment shows positive (negative) changes in the tropical (southeast) Pacific with high agreement between the different models, the aerosol forcing response exhibits an opposite response of similar magnitude, but with lower agreement between the different models (Figures 12i–12l). The relative strength of the forcing depends on the specific model in question. As a result, the historical response shows low agreement between models in those regions (Figures 12a–12d). By contrast, changes associated with ozone forcing are small in magnitude and mostly concentrated in the mid-to high latitudes during DJF only (Figures 12m–12p). During DJF, the response due to the ozone forcing generally resembles the response to GHG forcing in mid-to high latitudes but with lower magnitude, though with a somewhat more robust drying response over the mid-latitude Southern Ocean and wettening over South Africa and southeastern Australia. Moreover, these results support the claim that GHG forcing is primarily responsible for positive precipitation trends in southeastern South America (Vera & Díaz, 2015; Zhang et al., 2016), in contrast to previous studies that reported a major role for ozone forcing (e.g., Gonzalez et al., 2014). However, the period considered by Gonzalez et al. (2014) (1960–1999) was characterized by more severe ozone depletion, which could partly explain the incremental contribution of this forcing, a result confirmed in the LESFMIP simulations (see Section 3.5). Overall, these results enable us to evaluate some previous attempts to attribute long-term changes in precipitation that were based on fewer models or smaller ensembles for single forcing simulations. Additionally, we propose a greater role for aerosol forcing for SH subtropical rainfall than has been reported previously, which partially offsets the response to GHG forcing.

3.5. Ozone Recovery

Trends calculated over the 1980–2014 period combine the effects of both the ozone depletion era (1980–1999) and the subsequent stabilization or recovery phase (2000–2014) (e.g., Banerjee et al., 2020; Zambri et al., 2021). Therefore, analysis of the 1980–2014 period could be mixing ozone depletion and recovery signals. To isolate the effects of ozone depletion and recovery, we compare the trends from 2000 to 2014 with those from 1980 to 1999, when ozone depletion peaked. We focus on some of the SH features identified previously, where ozone forcing is relevant, and only consider DJF (austral summer), the season when ozone forcing has its largest influence. Direct comparisons between these two epochs (Figure 13) show a clear weakening in positive SAM trends in both reanalyses and the historical model ensemble during the later period (Figure 13a, e.g., Purich et al., 2026). A similar behavior is observed for the poleward shift of the Hadley cell edge; although the uncertainty in the reanalysis estimate is greater in this case, the large ensembles provide a clear sense of the robustness of this change. Regarding the FSW date (Figure 13c), both reanalyses and the models show a trend toward later FSWs over the 1980–1999 period, but a trend which has weakened or even reversed during 2000–2014 (note that the 2002 sudden stratospheric warming was removed from the reanalysis in the trend calculation). In line with the SAM changes, the positive trends in DJF extratropical precipitation in high latitudes (55°S–75°S) show a weakening in the later period (Figure 13d).

When comparing the historical experiment with the single-forcing experiments, it is clear that the simulated changes in trend magnitudes for these circulation metrics between the two periods come from ozone forcing. In particular, in the hist-totalO3 experiment, most of the metrics exhibit a reversal in the sign of the trend between the two periods (whereas in the historical experiment, only the FSW metric exhibits a reversal in sign; the other metrics show the same sign of trend but with reduced amplitude). On the other hand, the median trends in the

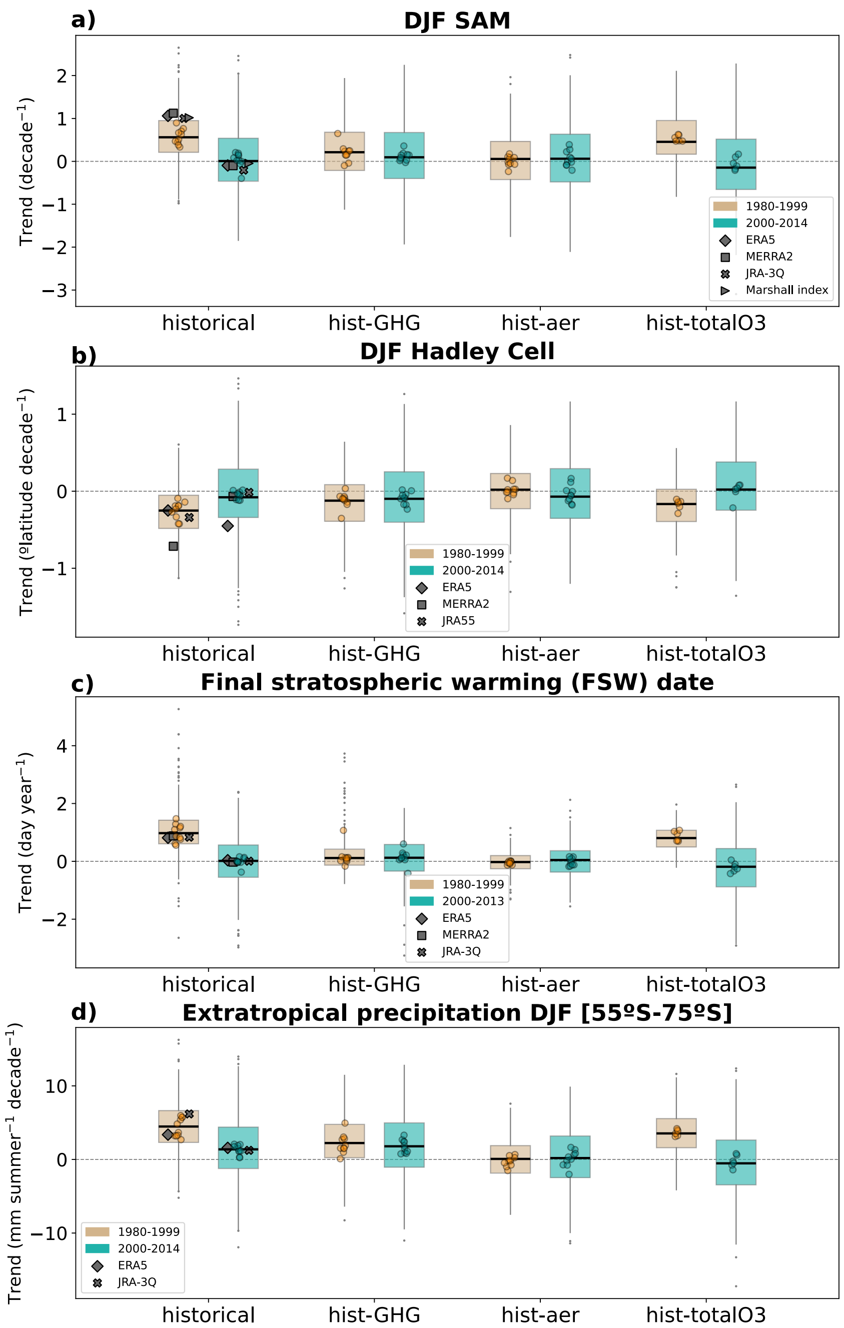

Figure 13. Box-and-whisker plot of the 1980–1999 and 2000–2014 linear trends for (a) SAM index, (b) SH Hadley Cell edge latitude, (c) final stratospheric warming date, and (d) extratropical precipitation (55°S–75°S) spatial average, for each experiment. All the individual simulations (independent of the model) are included for each box. In each case, the circles are the multi-model mean for each model. In the historical experiment, observational references are also included. For the FSW trends the period of 2000–2013 was used and the year 2002 was excluded in the reanalyses (see Figure 8).

aerosol single-forcing are around zero, for both of these two periods (aerosols had a larger effect relative to the preindustrial period, see e.g., Figures 6 and 7). Meanwhile, the GHG forcing shows no evident change between the two periods, so also cannot explain the inflection point in the historical evolution. These results suggest that the 1980–2014 trends shown in the previous sections for the historical and hist-totalO3 experiments may therefore represent a blend of accelerating trends during ozone depletion and weakening trends during ozone recovery for

Table 2
Summary of Observed Long-Term (1850–2014) SH Climate Changes and Associated Forcings Attributed to Them (in Brackets, Separated by a Comma in Order of Contribution, With a Slash Indicating Similar Contributions): GHG, Ozone (O3), Aerosols (AER)

Climate Variable/Metric	Summer (DJF)	Autumn (MAM)	Winter (JJA)	Spring (SON)
TOA Net Flux Imbalance—Annual	↑ (GHG, AER)			
Zonal Wind -Poleward Flank Jet Stream	↑ (GHG/O3)	↑ (GHG)	↑ (GHG)	↑ (GHG, O3)
Poleward shift of HC Edge Latitude	↑ (GHG, O3)	↑ (GHG)	↑ (GHG), ↓ (AER)	↑ (GHG), ↓ (AER)
SAM Index	↑ (GHG/O3), ↓ (AER)	↑ (GHG)	↑ (GHG)	↑ (GHG, O3), ↓ (AER)
FSW Date Delay	↑ (O3, GHG), ↓ (AER)			
SO SSTs—Annual	*↑ (GHG)*			
SO Air-Sea Heat Flux—Annual	↑ (GHG), ↓ (AER)			
Subsurface Ocean Temperatures Mid-latitudes—Annual	↑ (GHG, O3), ↓ (AER)			
Antarctic Sea Ice	Feb-Minimum: *↓ (GHG)*		Sep-Maximum: *↓ (GHG, O3)*	
Extratropical Precipitation (55°S–75°S)	↑ (GHG, O3)	↑ (GHG)	↑ (GHG)	↑ (GHG)

Note. Positive (negative) changes are indicated by (↑) (↓). Changes for which a discrepancy is found between models and observations for the 1980–2014 period using the criteria described in Section 2 are indicated in gray italics (where the changes indicated are those from the models, with observations showing an opposite-signed change). In each case, attribution forcings are indicated when the spread among models toward the end of the period (±1 standard deviation) is distinguishable from the preindustrial reference period.

some variables such as the SAM, the Hadley cell edge latitude, the FSW date, and precipitation changes, particularly during DJF.

These results support previous reports of early signals of ozone recovery in the circulation (Banerjee et al., 2020; Zambri et al., 2021; Zheng, 2024). However, those studies relied on observations or only a few models or ensemble members. Here, we confirm using single-forcing large ensembles that (a) observed changes in these circulation metrics during DJF in the early 21st century are within the range of simulated trends, which can vary substantially across ensemble members; (b) the ensemble-means of individual models and the MMM show robust changes between these two periods; and (c) the differences in circulation trends over these two time periods are driven by ozone forcing.

4. Discussion and Conclusion

The new LESFMIP simulations are the most complete set of multi-model single forcing experiments to date, with at least 10 members for each model and experiment. This allows us to revisit with a common framework the long-term changes (1980–2014 vs. 1850–1884) in the SH circulation and surface response, and their attribution to the main anthropogenic forcings: GHGs, ozone and aerosol forcing. The main long-term changes, the forcing factors that explain these changes, and the observation-model discrepancies found in our study are summarized in the following table (Table 2) and illustrative figure (Figure 14). It should be noted that these findings do not necessarily represent the results found for the shorter 1980–1999 and 2000–2014 periods, for which the effects of changing ozone forcing on the circulation approached or even exceeded those of GHGs in some seasons (see Section 3.5). Looking at the full record mixes together the ozone depletion and recovery signals.

Some of the key findings from this study, confirm and extend previous research:

- *Dominance of GHG forcing*: Our results highlight the predominant role of GHG forcing in explaining the simulated atmospheric and oceanic response in all-forcing historical experiments year-round over this ~170 year period.
- *Seasonal importance of ozone forcing*: Total column ozone forcing, which is dominated by stratospheric ozone depletion starting in the 1970s, exerts an influence on the SH atmospheric circulation that is comparable in magnitude, or for some metrics even larger than, the influence of GHGs, but only in certain seasons. In particular, in DJF (summer), ozone forcing exerts an equivalent magnitude influence to GHGs on the zonal-mean zonal winds (Figure 3), SLP (Figure 4), eddy-driven jet latitude (Figure S2 in Supporting Information S1) and SAM (Figure 6); and a slightly weaker but still substantial influence on the SH Hadley cell edge (Figure 5) and mid-to high-latitude precipitation (Figure 12). In SON (spring), ozone forcing also exerts an

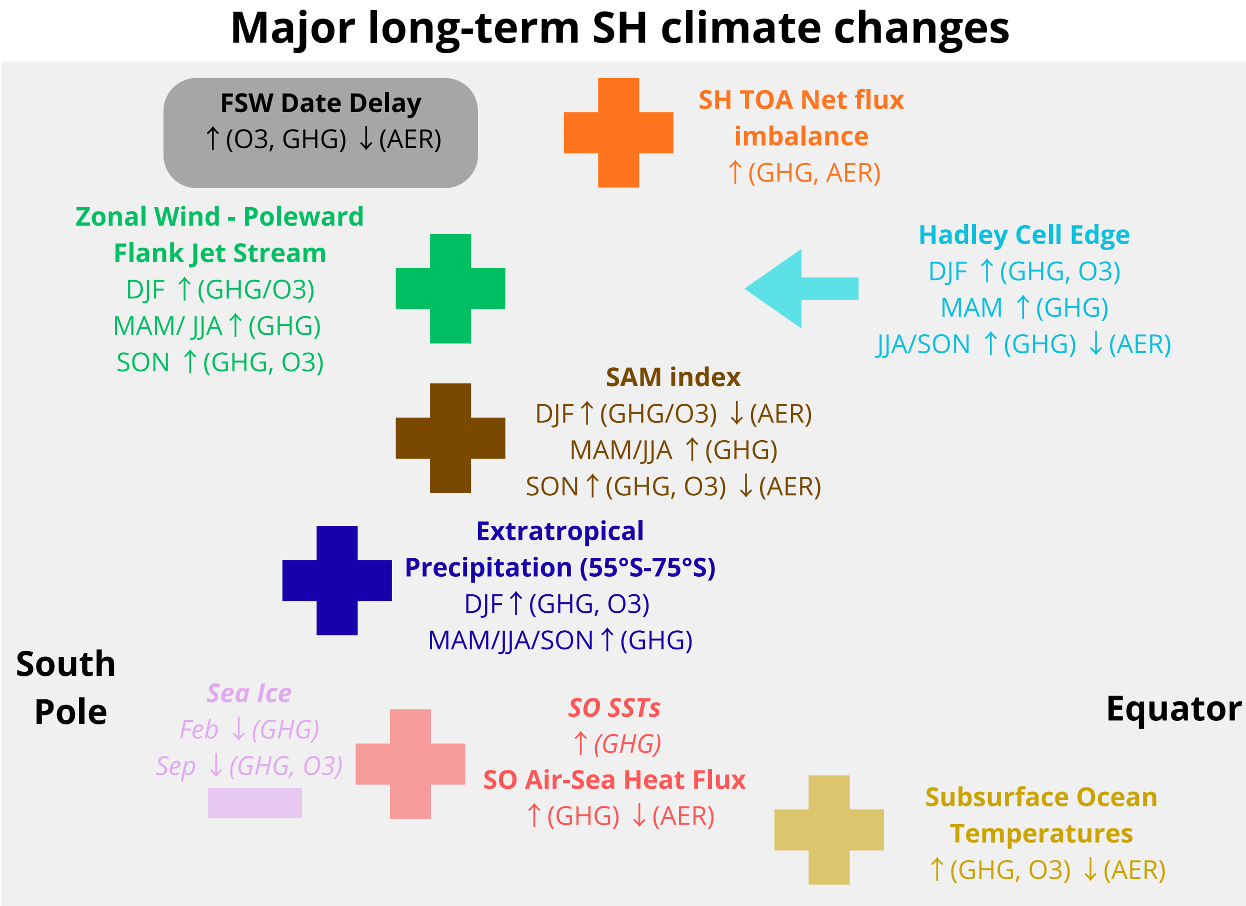

Figure 14. Summary of observed long-term (1850–2014) SH climate changes and associated forcings attributed to them (in brackets, separated by a comma in order of contribution, with a slash indicating similar contributions): GHG, ozone (O3), aerosols (AER). Positive (negative) changes are indicated by +(−) or by (↑) (↓). Poleward shifts are indicated by ←. Changes for which a discrepancy is found between models and observations for the 1980–2014 period using the criteria described in Section 2 are indicated in italic (where the changes indicated are those from the models, with observations showing an opposite-signed change). In each case, attribution forcings are indicated when the spread among models towards the end of the period is distinguishable from the preindustrial reference period.

equivalent influence to GHGs on stratospheric zonal winds (Figure 3), while being the primary driver of the FSW delay (Figure 7). Ozone forcing plays a weaker but still substantial role on springtime mean SLP, eddy-driven jet latitude, and SAM. Our results highlighted that ozone forcing may even provide some weak contribution to changes in circulation metrics in other seasons, such as mean SLP and the SAM in MAM (autumn) or polar stratospheric winds in JJA, though it is possible these changes are related to tropospheric, rather than stratospheric, ozone forcing.

- *Moderating role of aerosols*: Although the effects of anthropogenic aerosols on the SH circulation are generally smaller than those produced by other forcings, they have a noticeable impact on many of the features explored. Unlike ozone forcing which is primarily stratospheric and largest over the SH high latitudes, aerosol forcing is primarily tropospheric and largest in the NH. Nonetheless, impacts of aerosols were detected even in the SH stratosphere (Figures 3 and 7). The zonal-mean atmospheric circulation response to aerosol forcing broadly opposes that to GHG, but with weaker magnitude. This is reflected in the simulated historical changes to the latitude of the SH Hadley cell edge (Figure 5), the position of the eddy-driven jet (Figure S2 in Supporting Information S1), the SAM index (Figure 6) and the FSW date (Figure 7). Additionally, the aerosol forcing partially offsets the simulated positive changes in Southern Ocean air-sea heat flux (Figure 8) and SH surface and deep ocean temperatures driven by GHG forcing (Figures 9 and 10), though its impact on SIE is negligible (Figure 11). Regarding the precipitation response, its impact in the South Pacific Ocean is comparable to that of GHG, but of opposite sign (Figure 12). Although the counteracting influence of aerosols was generally present year-round, in some cases it was present only in particular seasons; for example, aerosols had a detectable influence on the SH Hadley cell edge extent only in JJA and SON. Our analysis highlights the importance of taking aerosol forcing into account when conducting attribution analyses, in order to obtain a realistic representation of the full anthropogenic climate response in the SH. Due to the reversal of global trends in aerosol emissions (Quaas et al., 2022), the counteracting effect of the aerosol forcing in the SH climate response may become weaker in the future.

We also identified discrepancies between observation-based data sets and the model simulations over 1980–2014. For example, we highlighted the contrast between the negative trend observed in Southern Ocean SSTs and the positive trends simulated by the models (Figure 8b), as well as the positive trend observed in sea ice extent that contrasts with simulated negative trends (Figure 11). Although these observation-model discrepancies have been reported previously (e.g., Simpson et al., 2025), our study includes a considerably larger number of individual simulations from different models than most previous studies. Therefore, we could confirm which discrepancies are much more likely to be genuine and not the result of insufficient sampling of internal variability, over the short observational period, by determining where the observations are well outside the model distribution. Where few models have individual members that closely match observed trends suggests a lack of physical understanding of the processes underlying these discrepancies, as well as a need for model development efforts aimed at improving the representation of these long-term features. Advances in both aspects would help to reduce uncertainties of future projections.

A novel component of our analysis is evaluating all four seasons to identify seasonal dependencies in long-term circulation trends and their causes. For instance, although our study confirms that DJF and to a lesser extent SON are the seasons when the many prominent SH circulation trends have emerged, the results also highlight that these seasons have been dominated by same-signed contributions from GHGs and ozone depletion; but in the future, ozone recovery and GHGs will instead have an opposite-signed influence, potentially leading to weaker and more uncertain SH circulation responses in these seasons compared to other seasons. On the other hand, MAM shows a long-term response similar to that of DJF, but with a slightly smaller magnitude, mostly attributable to GHG forcing. This is mainly due to the lack of ozone forcing in this season compared with SON and DJF, which may imply MAM will become a better season to detect future changes in the circulation. Our results show that the observed circulation trends in MAM (Figures 5 and 6; Figure S2 in Supporting Information S1) are much larger than the trends indicated by the model ensemble mean. Although this could be a result of internal variability over this shorter period, attention should be given to the models' ability to correctly capture the amplitude of the response to forcing in this season, as this is the season in which we expect forced changes to become most apparent in the next few decades. Additionally, our analysis identified some previously unidentified responses in certain seasons; for example, ozone forcing was found to lead to a robust weakening on the poleward flank of the winter polar vortex, motivating further study into the causes for these changes.

The ozone-only forcing simulations also allow us to evaluate the extent to which the recovery of stratospheric ozone, due to actions under the Montreal Protocol, has a detectable signature in SH circulation trends and related surface impacts. We clearly identified that some of the main long-term changes in the SH during DJF, such as the SAM positive trend, the poleward shift in the latitude of the Hadley cell edge, the delay in the FSW and the positive precipitation trend at high latitudes, are considerably diminishing in the large ensembles, with a clear slowdown during 2000–2014 relative to 1980–1999 in the historical and ozone forcing simulations (Figure 13). We also used the LESFMIP simulations to investigate the hypothesis put forth by Hartmann (2022) and Dong et al. (2025), who suggested that ozone depletion has contributed to the observed tropical La Niña-like cooling pattern in SSTs. Using multi-model large ensembles, we see robust regional SST cooling in the southeastern Pacific and Southern Ocean due to ozone forcing in DJF, with higher model agreement during the peak period of ozone depletion (Figure S4 in Supporting Information S1), though it is not possible to conduct a direct comparison with Dong et al. (2025) due to differences in ozone forcing. This suggests that further exploration of the connection between ozone forcing and SSTs is warranted.

There are a few important caveats to our results. One limitation is that the LESFMIP model simulations do not permit a fair comparison with most previous studies, since the LESFMIP ozone-only forcing includes both tropospheric and stratospheric ozone. This differs from the stratospheric-only ozone forcing commonly used in previous studies (e.g., Gillett et al., 2016). An additional caveat is that none of the LESFMIP models incorporate interactive ozone chemistry. Prescribed ozone has been shown to result in weaker stratospheric responses to changes in ozone levels (depletion and subsequent recovery), which could lead to underestimation of the long-term responses of ozone forcing compared to GHG (Butler et al., 2026; Ivanciu et al., 2021, 2022). Generating simulations that allow the role of interactive chemistry to be evaluated using a large ensemble approach involving multiple models would improve our understanding of the comparative roles of GHG and ozone forcings in explaining the response of SH circulation and its associated impacts. Another source of uncertainty arose from the aerosol forcing used in the LESFMIP simulations, as previous studies have shown that CMIP model simulations are highly sensitive to plausible historical aerosol forcings (e.g., Dittus et al., 2020; Fyfe et al., 2021). Therefore, the contribution of aerosol forcing suggested by our results remains highly uncertain.

Although it was not shown in our analysis, we found evidence of a non-additive response in the circulation changes across different forcing agents (e.g., DJF SH Hadley cell edge latitude, Figure 5). Recently, Pope et al. (2020) reported differences in the SH SLP response when combining GHGs and aerosols, compared to the sum of the individual forcings, using a coupled chemistry–climate model. In addition, Simpson et al. (2023) identified significant nonlinearities in the response of Atlantic meridional overturning circulation for anthropogenic aerosol forcing by comparing the results of the "only" and "all-but-one" methods used in the design of single-forcing experiments. Further research is required to establish the importance of such nonlinearities in order to understand the limitations of attributing specific forcing agents to single-forcing simulations in the SH changes. Another issue that requires more attention is the long-term change in interannual variability, as our study primarily focuses on long-term changes in mean circulation. This could be particularly important for understanding climate extremes and predictability, and improving the physical interpretation of climate projections. Large ensembles are an ideal tool for investigating these aspects (Deser et al., 2020; Maher et al., 2021). Butler et al. (2026) recently considered a smaller set of large ensembles and found that the dominant mode of variability in SH stratosphere-troposphere coupling changes in response to external forcings, with higher variability shifting to early summer as ozone depletion peaks and back to spring as ozone recovery occurs, and variability of the mode decreasing by the end of the 21st century. LESFMIP simulations may prove a useful tool for future evaluation of the long-term evolution of SH circulation variability and its potential causes.

Although our assessment mainly focuses on signals where all models show agreement, we acknowledge that using equal weights for individual model ensemble means does not address that some models may have larger biases than others, nor do we attempt to systematically evaluate models in order to better constrain the simulations to represent the actual evolution of the long-term climate. Furthermore, despite using large ensembles, our results could be impacted by signal-to-noise errors, which could result in the magnitude of the modelled ensemble mean and spread appearing smaller than it actually is (Cottrell et al., 2024; Scaife & Smith, 2018). This could be addressed by scaling the simulated response by the ratio of predictable signals between observations and simulations. However, this is more complicated if models have different responses, and a reliable observational reference is still needed for this computation, which is not always possible for SH circulation variables. Recent efforts to exploit model differences to explain and predict long-term climate evolution include the work of Smith et al. (2025), who developed an emergent constraint based on climatological water vapor errors to predict the evolution of the North Atlantic Oscillation over multiple decades using CMIP6 and LESFMIP experiments. Alternatively, Mindlin et al. (2025) developed a causal framework combining observation-based data sets and storylines estimated from CMIP6 simulations to attribute DJF eddy-driven jet changes and predict plausible future trajectories. A key process to evaluate is the accurate representation of the Southern Ocean, where observation-model discrepancies are substantial (Section 3.3). As pointed out by Yeager et al. (2023), improving representation of the Southern Ocean is critical for improving long-term climate change simulations in climate models, as well as potentially improving decadal climate predictions. Further work will be conducted to understand and exploit model differences, using LESFMIP simulations to gain a deeper understanding of long-term SH circulation trends. These analyses could help constrain the expected future evolution of the climate, depending on the scenario.

Conflict of Interest

The authors declare no conflicts of interest relevant to this study.

Availability Statement

All simulation data used in this study is available on the Earth System Grid Federation (ESGF; https://aims2.llnl.gov/search; Cinquini et al., 2014). The fifth generation ECMWF atmospheric reanalysis (ERA5) can be downloaded from the Climate Data Store from Copernicus (https://cds.climate.copernicus.eu/datasets) and is referenced in the text as Hersbach et al. (2020). The Modern-Era Retrospective analysis for Research and Applications, Version 2 (MERRA2) can be downloaded from NASA Goddard Earth Sciences Data and Information Services Center (DISC) (https://disc.gsfc.nasa.gov/datasets?project=MERRA-2) and is referenced in the text as Gelaro et al. (2017). The Japanese 55-year Reanalysis (JRA-55) can be downloaded from the NSF NCAR Geoscience Data Exchange (https://gdex.ucar.edu/datasets/d628001/) and is referenced in the text as Kobayashi et al. (2015). The Japanese Reanalysis for Three Quarters of a Century (JRA-3Q) can be downloaded from the NSF NCAR Geoscience Data Exchange (https://gdex.ucar.edu/datasets/d640002/dataaccess/) and is referenced in the text as Kosaka et al. (2024). The Extended Reconstructed Sea Surface Temperature, Version 5 (ERSSTv5) can be downloaded from the NOAA Physical Sciences Laboratory (https://psl.noaa.gov/data/gridded/data.noaa.ersst.v5.html) and is referenced in the text as Huang et al. (2017). The EUMETSAT Ocean and Sea Ice Satellite Application Facility (OSI SAF) can be downloaded from the Copernicus Marine Service (https://data.marine.copernicus.eu/product/SEAICE_GLO_SEAICE_L4_REP_OBSERVATIONS_011_009/services) and is referenced in the text as Lavergne et al. (2019). The observational (station)-based SAM index can be downloaded from https://legacy.bas.ac.uk/met/gjma/sam.html and is referenced in the text as Marshall (2003). This work used JASMIN, the UK's collaborative data analysis environment (https://www.jasmin.ac.uk; Lawrence et al., 2013).

Acknowledgments

We acknowledge the support from the World Climate Research Programme (WCRP) Lighthouse Activity on Explaining and Predicting Earth System Change (EPESC) and the Large Ensembles for Attribution of Dynamically driven ExtRemes (LEADER) activity from the WCRP Core Project Atmospheric Processes And their Role in Climate (APARC). LBD and MO were supported by the Universidad de Buenos Aires (Grant UBACyT20020220100075BA) and CONICET (Grant CONICET-PIP 11220200102038CO). GB and EL were supported by the National Environmental Science Program (NESP), funded by the Australian Department of Climate Change, Energy, the Environment and Water. HK was supported by the Met Office Hadley Centre Climate Programme funded by DSIT. BM carried out the analysis as a Fonds de la Recherche Scientifique—FNRS (F.R.S.–FNRS) postdoctoral researcher. TB and SO would like to acknowledge support from the UK NERC CANARI program (NE/W004984/1). SO was funded by the UK NERC AUSPICE project (UKRI2165). GB, EL and JMA were supported by the Australian Research Council Special Research Initiative for Securing Antarctica's Environmental Future (SAEF) Program (SR200100005).

References

Adam, O., Grise, K. M., Staten, P., Simpson, I. R., Davis, S. M., Davis, N. A., et al. (2018). The TropD software package (v1): Standardized methods for calculating tropical-width diagnostics. *Geoscientific Model Development*, *11*(10), 4339–4357. https://doi.org/10.5194/gmd-11-4339-2018

Allen, R. J., & Kovilakam, M. (2017). The role of natural climate variability in recent tropical expansion. *Journal of Climate*, *30*(16), 6329–6350. https://doi.org/10.1175/JCLI-D-16-0735.1

Arblaster, J. M., & Meehl, G. A. (2006). Contributions of external forcings to southern annular mode trends. *Journal of Climate*, *19*(12), 2896–2905. https://doi.org/10.1175/JCLI3774.1

Arblaster, J. M., Meehl, G. A., & Karoly, D. J. (2011). Future climate change in the Southern Hemisphere: Competing effects of ozone and greenhouse gases. *Geophysical Research Letters*, *38*(2). https://doi.org/10.1029/2010GL045384

Auger, M., Morrow, R., Kestenare, E., Sallée, J.-B., & Cowley, R. (2021). Southern Ocean in-situ temperature trends over 25 years emerge from interannual variability. *Nature Communications*, *12*(1), 514. https://doi.org/10.1038/s41467-020-20781-1

Bandoro, J., Solomon, S., Donohoe, A., Thompson, D. W. J., & Santer, B. D. (2014). Influences of the Antarctic ozone hole on southern hemispheric summer climate change. *Journal of Climate*, *27*(16), 6245–6264. https://doi.org/10.1175/JCLI-D-13-00698.1

Banerjee, A., Fyfe, J. C., Polvani, L. M., Waugh, D., & Chang, K.-L. (2020). A pause in Southern Hemisphere circulation trends due to the Montreal protocol. *Nature*, *579*(7800), 544–548. https://doi.org/10.1038/s41586-020-2120-4

Bitz, C. M., & Polvani, L. M. (2012). Antarctic climate response to stratospheric ozone depletion in a fine resolution ocean climate model. *Geophysical Research Letters*, *39*(20). https://doi.org/10.1029/2012GL053393

Boisier, J. P., Alvarez-Garreton, C., Cordero, R. R., Damiani, A., Gallardo, L., Garreaud, R. D., et al. (2018). Anthropogenic drying in central-southern Chile evidenced by long-term observations and climate model simulations. *Elementa: Science of the Anthropocene*, *6*, 74. https://doi.org/10.1525/elementa.328

Boucher, O., Servonnat, J., Albright, A. L., Aumont, O., Balkanski, Y., Bastrikov, V., et al. (2020). Presentation and evaluation of the IPSL-CM6A-LR climate model. *Journal of Advances in Modeling Earth Systems*, *12*(7), e2019MS002010. https://doi.org/10.1029/2019MS002010

Brönnimann, S., Jacques-Coper, M., Rozanov, E., Fischer, A. M., Morgenstern, O., Zeng, G., et al. (2017). Tropical circulation and precipitation response to ozone depletion and recovery. *Environmental Research Letters*, *12*(6), 064011. https://doi.org/10.1088/1748-9326/aa7416

Butler, A. H., & Domeisen, D. I. V. (2021). The wave geometry of final stratospheric warming events. *Weather and Climate Dynamics*, *2*, 453–474. https://doi.org/10.5194/wcd-2-453-2021

Butler, A. H., Lim, E.-P., & Simpson, I. R. (2026). Externally-forced changes to Southern Hemisphere stratosphere-troposphere coupling variability. *Earth's Future*, *14*(3), e2025EF007334. https://doi.org/10.1029/2025EF007334

Byrne, N. J., & Shepherd, T. G. (2018). Seasonal persistence of circulation anomalies in the Southern Hemisphere stratosphere and its implications for the troposphere. *Journal of Climate*, *31*(9), 3467–3483. https://doi.org/10.1175/JCLI-D-17-0557.1

Cai, W., & Cowan, T. (2013). Southeast Australia autumn rainfall reduction: A climate-change-induced poleward shift of ocean–atmosphere circulation. *Journal of Climate*, *26*(1), 189–205. https://doi.org/10.1175/JCLI-D-12-00035.1

Cai, W., Cowan, T., & Thatcher, M. (2012). Rainfall reductions over Southern Hemisphere semi-arid regions: The role of subtropical dry zone expansion. *Scientific Reports*, *2*(1), 702. https://doi.org/10.1038/srep00702

Cai, W., Gao, L., Luo, Y., Li, X., Zheng, X., Zhang, X., et al. (2023). Southern Ocean warming and its climatic impacts. *Science Bulletin*, *68*(9), 946–960. https://doi.org/10.1016/j.scib.2023.03.049

Cao, J., Lian, X., Cao, M., Wang, B., Wang, H., Zhu, X., & Zhao, H. (2023). Wettening of the Southern Hemisphere land monsoon during 1901–2014. *Journal of Climate*, *36*(24), 8497–8512. https://doi.org/10.1175/JCLI-D-23-0066.1

Casagrande, F., Stachelski, L., & de Souza, R. B. (2023). Assessment of Antarctic sea ice area and concentration in coupled model intercomparison project phase 5 and phase 6 models. *International Journal of Climatology*, *43*(3), 1314–1332. https://doi.org/10.1002/joc.7916

Checa-Garcia, R., Hegglin, M. I., Kinnison, D., Plummer, D. A., & Shine, K. P. (2018). Historical tropospheric and stratospheric ozone radiative forcing using the CMIP6 database. *Geophysical Research Letters*, *45*(7), 3264–3273. https://doi.org/10.1002/2017GL076770

Chemke, R., Ming, Y., & Yuval, J. (2022). The intensification of winter mid-latitude storm tracks in the Southern Hemisphere. *Nature Climate Change*, *12*(6), 553–557. https://doi.org/10.1038/s41558-022-01368-8

Chen, J.-J., Swart, N. C., & Cheng, X. (2022). Processes controlling the southern ocean temperature change. *Journal of Climate*, *35*(23), 7739–7749. https://doi.org/10.1175/JCLI-D-22-0111.1

Choi, J., Son, S.-W., & Park, R. J. (2019). Aerosol versus greenhouse gas impacts on Southern Hemisphere general circulation changes. *Climate Dynamics*, *52*(7), 4127–4142. https://doi.org/10.1007/s00382-018-4370-5

Chou, H.-H., Shaw, T. A., & Zhang, G. (2025). Human influence on recent trends in extratropical low-level wind speed. *npj Climate and Atmospheric Science*, *9*(1), 20. https://doi.org/10.1038/s41612-025-01292-6

Cinquini, L., Crichton, D., Mattmann, C., Harney, J., Shipman, G., Wang, F., et al. (2014). The Earth system grid Federation: An open infrastructure for access to distributed geospatial data [Dataset]. *Future Generation Computer Systems*, *36*, 400–417. https://doi.org/10.1016/j.future.2013.07.002

Cottrell, F. M., Screen, J. A., & Scaife, A. A. (2024). Signal-to-noise errors in free-running atmospheric simulations and their dependence on model resolution. *Atmospheric Science Letters*, *25*(6), e1212. https://doi.org/10.1002/asl.1212

Delworth, T. L., & Zeng, F. (2014). Regional rainfall decline in Australia attributed to anthropogenic greenhouse gases and ozone levels. *Nature Geoscience*, *7*(8), 583–587. https://doi.org/10.1038/ngeo2201

Deser, C., Lehner, F., Rodgers, K. B., Ault, T., Delworth, T. L., DiNezio, P. N., et al. (2020). Insights from Earth system model initial-condition large ensembles and future prospects. *Nature Climate Change*, *10*(4), 277–286. https://doi.org/10.1038/s41558-020-0731-2

Díaz, L. B., Saurral, R. I., & Vera, C. S. (2021). Assessment of South America summer rainfall climatology and trends in a set of global climate models large ensembles. *International Journal of Climatology*, *41*(S1), E59–E77. https://doi.org/10.1002/joc.6643

Dittus, A. J., Hawkins, E., Wilcox, L. J., Sutton, R. T., Smith, C. J., Andrews, M. B., & Forster, P. M. (2020). Sensitivity of historical climate simulations to uncertain aerosol forcing. *Geophysical Research Letters*, *47*(13), e2019GL085806. https://doi.org/10.1029/2019GL085806

Dong, Y., Polvani, L. M., & Bonan, D. B. (2023). Recent multi-decadal Southern Ocean surface cooling unlikely caused by southern annular mode trends. *Geophysical Research Letters*, *50*(23), e2023GL106142. https://doi.org/10.1029/2023GL106142

Dong, Y., Polvani, L. M., Hwang, Y. T., & England, M. R. (2025). Stratospheric ozone depletion has contributed to the recent tropical La Niña-like cooling pattern. *npj Climate and Atmospheric Science*, *8*(1), 150. https://doi.org/10.1038/s41612-025-01020-0

Eayrs, C., Li, X., Raphael, M. N., & Holland, D. M. (2021). Rapid decline in Antarctic sea ice in recent years hints at future change. *Nature Geoscience*, *14*(7), 460–464. https://doi.org/10.1038/s41561-021-00768-3

Eyring, V., Arblaster, J. M., Cionni, I., Sedláček, J., Perlwitz, J., Young, P. J., et al. (2013). Long-term ozone changes and associated climate impacts in CMIP5 simulations. *Journal of Geophysical Research: Atmospheres*, *118*(10), 5029–5060. https://doi.org/10.1002/jgrd.50316

Eyring, V., Bony, S., Meehl, G. A., Senior, C. A., Stevens, B., Stouffer, R. J., & Taylor, K. E. (2016). Overview of the coupled model intercomparison project phase 6 (CMIP6) experimental design and organization. *Geoscientific Model Development*, *9*(5), 1937–1958. https://doi.org/10.5194/gmd-9-1937-2016

Ferreira, D., Marshall, J., Bitz, C. M., Solomon, S., & Plumb, A. (2015). Antarctic Ocean and sea ice response to ozone depletion: A two-time-scale problem. *Journal of Climate*, *28*(3), 1206–1226. https://doi.org/10.1175/JCLI-D-14-00313.1

Fiedler, S., Kinne, S., Huang, W. T. K., Räisänen, P., O'Donnell, D., Bellouin, N., et al. (2019). Anthropogenic aerosol Forcing – Insights from multiple estimates from aerosol-climate models with reduced complexity. *Atmospheric Chemistry and Physics*, *19*(10), 6821–6841. https://doi.org/10.5194/acp-19-6821-2019

Findell, K. L., Sutton, R., Caltabiano, N., Brookshaw, A., Heimbach, P., Kimoto, M., et al. (2023). Explaining and predicting Earth system change: A world climate research programme call to action. *Bulletin of the American Meteorological Society*, *104*(1), E325–E339. https://doi.org/10.1175/BAMS-D-21-0280.1

Fogt, R. L., & Marshall, G. J. (2020). The southern annular mode: Variability, trends, and climate impacts across the Southern Hemisphere. *WIREs Climate Change*, *11*(4), e652. https://doi.org/10.1002/wcc.652

Fyfe, J. C., Gillett, N. P., & Marshall, G. J. (2012). Human influence on extratropical Southern Hemisphere summer precipitation. *Geophysical Research Letters*, *39*(23). https://doi.org/10.1029/2012GL054199

Fyfe, J. C., Kharin, V. V., Santer, B. D., Cole, J. N. S., & Gillett, N. P. (2021). Significant impact of forcing uncertainty in a large ensemble of climate model simulations. *Proceedings of the National Academy of Sciences*, *118*(23), e2016549118. https://doi.org/10.1073/pnas.2016549118

Garfinkel, C. I., Waugh, D. W., & Polvani, L. M. (2015). Recent Hadley cell expansion: The role of internal atmospheric variability in reconciling modeled and observed trends. *Geophysical Research Letters*, *42*(24), 10824–10831. https://doi.org/10.1002/2015GL066942

Gelaro, R., McCarty, W., Suárez, M. J., Todling, R., Molod, A., Takacs, L., et al. (2017). The modern-era retrospective analysis for research and applications, version 2 (MERRA-2) [Dataset]. *Journal of Climate*, *30*(14), 5419–5454. https://doi.org/10.1175/JCLI-D-16-0758.1

Gillett, N. P., Fyfe, J. C., & Parker, D. E. (2013). Attribution of observed sea level pressure trends to greenhouse gas, aerosol, and ozone changes. *Geophysical Research Letters*, *40*(10), 2302–2306. https://doi.org/10.1002/grl.50500

Gillett, N. P., Kirchmeier-Young, M., Ribes, A., Shiogama, H., Hegerl, G. C., Knutti, R., et al. (2021). Constraining human contributions to observed warming since the pre-industrial period. *Nature Climate Change*, *11*(3), 207–212. https://doi.org/10.1038/s41558-020-00965-9

Gillett, N. P., Shiogama, H., Funke, B., Hegerl, G., Knutti, R., Matthes, K., et al. (2016). The detection and attribution model intercomparison project (DAMIP v1.0) contribution to CMIP6. *Geoscientific Model Development*, *9*(10), 3685–3697. https://doi.org/10.5194/gmd-9-3685-2016

Gillett, N. P., Simpson, I. R., Hegerl, G., Knutti, R., Mitchell, D., Ribes, A., et al. (2025). The detection and attribution model intercomparison project (DAMIP v2.0) contribution to CMIP7. *Geoscientific Model Development*, *18*(14), 4399–4416. https://doi.org/10.5194/gmd-18-4399-2025

Gillett, N. P., & Thompson, D. W. J. (2003). Simulation of recent Southern Hemisphere climate change. *Science*, *302*(5643), 273–275. https://doi.org/10.1126/science.1087440

Gong, D., & Wang, S. (1999). Definition of Antarctic oscillation index. *Geophysical Research Letters*, *26*(4), 459–462. https://doi.org/10.1029/1999GL900003

Gonzalez, P. L. M., Polvani, L. M., Seager, R., & Correa, G. J. P. (2014). Stratospheric ozone depletion: A key driver of recent precipitation trends in South Eastern South America. *Climate Dynamics*, *42*(7), 1775–1792. https://doi.org/10.1007/s00382-013-1777-x

Grise, K. M., & Davis, S. M. (2020). Hadley cell expansion in CMIP6 models. *Atmospheric Chemistry and Physics*, *20*(9), 5249–5268. https://doi.org/10.5194/acp-20-5249-2020

Grise, K. M., Davis, S. M., Simpson, I. R., Waugh, D. W., Fu, Q., Allen, R. J., et al. (2019). Recent tropical expansion: Natural variability or forced response? *Journal of Climate*, *32*(5), 1551–1571. https://doi.org/10.1175/JCLI-D-18-0444.1

Grise, K. M., Davis, S. M., Staten, P. W., & Adam, O. (2018). Regional and seasonal characteristics of the recent expansion of the tropics. *Journal of Climate*, *31*(17), 6839–6856. https://doi.org/10.1175/JCLI-D-18-0060.1

Grise, K. M., & Polvani, L. M. (2017). Understanding the time scales of the tropospheric circulation response to abrupt CO2 forcing in the Southern Hemisphere: Seasonality and the role of the stratosphere. *Journal of Climate*, *30*, 8497–8515. https://doi.org/10.1175/JCLI-D-16-0849.1

Grise, K. M., Son, S.-W., Correa, G. J. P., & Polvani, L. M. (2014). The response of extratropical cyclones in the Southern Hemisphere to stratospheric ozone depletion in the 20th century. *Atmospheric Science Letters*, *15*(1), 29–36. https://doi.org/10.1002/asl2.458

Gulev, S. K., Thorne, P. W., Ahn, J., Dentener, F. J., Domingues, C. M., Gerland, S., et al. (2021). Changing state of the climate system. In V. Masson-Delmotte, P. Zhai, A. Pirani, S. L. Connors, C. Péan, S. Berger, et al. (Eds.), *Climate change 2021: The physical science basis. Contribution of working group I to the sixth assessment report of the intergovernmental panel on climate change* (pp. 287–422). Cambridge University Press. https://doi.org/10.1017/9781009157896.004

Haase, S., Fricke, J., Kruschke, T., Wahl, S., & Matthes, K. (2020). Sensitivity of the Southern Hemisphere circumpolar jet response to Antarctic ozone depletion: Prescribed versus interactive chemistry. *Atmospheric Chemistry and Physics*, *20*(22), 14043–14061. https://doi.org/10.5194/acp-20-14043-2020

Hardiman, S. C., Butchart, N., Charlton-Perez, A. J., Shaw, T. A., Akiyoshi, H., Baumgaertner, A., et al. (2011). Improved predictability of the troposphere using stratospheric final warmings. *Journal of Geophysical Research*, *116*(D18), D18113. https://doi.org/10.1029/2011JD015914

Hartmann, D. L. (2022). The Antarctic ozone hole and the pattern effect on climate sensitivity. *Proceedings of the National Academy of Sciences*, *119*(35), e2207889119. https://doi.org/10.1073/pnas.2207889119

Heidemann, H., Cowan, T., Henley, B. J., Ribbe, J., Freund, M., & Power, S. (2023). Variability and long-term change in Australian monsoon rainfall: A review. *WIREs Climate Change*, *14*(3), e823. https://doi.org/10.1002/wcc.823

Hendon, H. H., Lim, E.-P., & Nguyen, H. (2014). Seasonal variations of subtropical precipitation associated with the southern annular mode. *Journal of Climate*, *27*(9), 3446–3460. https://doi.org/10.1175/JCLI-D-13-00550.1

Hendon, H. H., Thompson, D. W. J., & Wheeler, M. C. (2007). Australian rainfall and surface temperature variations associated with the Southern Hemisphere annular mode. *Journal of Climate*, *20*(11), 2452–2467. https://doi.org/10.1175/JCLI4134.1

Hersbach, H., Bell, B., Berrisford, P., Hirahara, S., Horányi, A., Muñoz-Sabater, J., et al. (2020). The ERA5 global reanalysis [Dataset]. *Quarterly Journal of the Royal Meteorological Society*, *146*(730), 1999–2049. https://doi.org/10.1002/qj.3803

Holland, M. M., Landrum, L., Kostov, Y., & Marshall, J. (2017). Sensitivity of Antarctic sea ice to the southern annular mode in coupled climate models. *Climate Dynamics*, *49*(5), 1813–1831. https://doi.org/10.1007/s00382-016-3424-9

Holmes, C. R., Bracegirdle, T. J., Holland, P. R., Stroeve, J., & Wilkinson, J. (2024). Brief communication: New perspectives on the skill of modelled sea ice trends in light of recent Antarctic sea ice loss. *The Cryosphere*, *18*(12), 5641–5652. https://doi.org/10.5194/tc-18-5641-2024

Huang, B., Thorne, P. W., Banzon, V. F., Boyer, T., Chepurin, G., Lawrimore, J. H., et al. (2017). Extended reconstructed sea surface temperature, version 5 (ERSSTv5): Upgrades, validations, and intercomparisons [Dataset]. *Journal of Climate*, *30*(20), 8179–8205. https://doi.org/10.1175/JCLI-D-16-0836.1

Hwang, Y.-T., Xie, S.-P., Chen, P.-J., Tseng, H.-Y., & Deser, C. (2024). Contribution of anthropogenic aerosols to persistent La Niña-like conditions in the early 21st century. *Proceedings of the National Academy of Sciences*, *121*(5), e2315124121. https://doi.org/10.1073/pnas.2315124121

IPCC. (2021). Summary for policymakers. In: Climate change 2021: The physical science basis. In V. Masson-Delmotte, P. Zhai, A. Pirani, S. L. Connors, C. Péan, et al. (Eds.), *Contribution of working group I to the sixth assessment report of the intergovernmental panel on climate change* (pp. 3–32). Cambridge University Press. https://doi.org/10.1017/9781009157896.001

Ivanciu, I., Matthes, K., Biastoch, A., Wahl, S., & Harlaß, J. (2022). Twenty-first-century Southern Hemisphere impacts of ozone recovery and climate change from the stratosphere to the ocean. *Weather and Climate Dynamics*, *3*(1), 139–171. https://doi.org/10.5194/wcd-3-139-2022

Ivanciu, I., Matthes, K., Wahl, S., Harlaß, J., & Biastoch, A. (2021). Effects of prescribed CMIP6 ozone on simulating the Southern Hemisphere atmospheric circulation response to ozone depletion. *Atmospheric Chemistry and Physics*, *21*(8), 5777–5806. https://doi.org/10.5194/acp-21-5777-2021

Jiang, F., Seager, R., & Cane, M. A. (2024). A climate change signal in the tropical Pacific emerges from decadal variability. *Nature Communications*, *15*(1), 8291. https://doi.org/10.1038/s41467-024-52731-6

Johanson, C. M., & Fu, Q. (2009). Hadley cell widening: Model simulations versus observations. *Journal of Climate*, *22*(10), 2713–2725. https://doi.org/10.1175/2008JCLI2620.1

Jones, G. S., Andrews, M. B., Andrews, T., Blockley, E., Ciavarella, A., Christidis, N., et al. (2024). The HadGEM3-GC3.1 contribution to the CMIP6 detection and attribution model intercomparison project. *Journal of Advances in Modeling Earth Systems*, *16*(8), e2023MS004135. https://doi.org/10.1029/2023MS004135

Kang, S. M., Ceppi, P., Yu, Y., & Kang, I.-S. (2023). Recent global climate feedback controlled by Southern Ocean cooling. *Nature Geoscience*, *16*(9), 775–780. https://doi.org/10.1038/s41561-023-01256-6

Kang, S. M., Polvani, L. M., Fyfe, J. C., & Sigmond, M. (2011). Impact of polar ozone depletion on subtropical precipitation. *Science*, *332*(6032), 951–954. https://doi.org/10.1126/science.1202131

Kang, S. M., Putrasahan, D. A., Brizuela, N. G., Haak, H., Kröger, J., Marotzke, J., et al. (2026). Km-scale coupled simulation and model–observation SST trend discrepancy. *Proceedings of the National Academy of Sciences*, *123*(8), e2522161123. https://doi.org/10.1073/pnas.2522161123

Karpechko, A. Y., Gillett, N. P., Gray, L. J., & Dall'Amico, M. (2010). Influence of ozone recovery and greenhouse gas increases on Southern Hemisphere circulation. *Journal of Geophysical Research*, *115*(D22). https://doi.org/10.1029/2010JD014423

Kaufman, Z., Wilson, E., Purich, A., Beadling, R., & Li, Y. (2025). The impact of underestimated southern ocean freshening on simulated historical sea surface temperature trends. *Geophysical Research Letters*, *52*(6), e2024GL112639. https://doi.org/10.1029/2024GL112639

Keeble, J., Braesicke, P., Abraham, N. L., Roscoe, H. K., & Pyle, J. A. (2014). The impact of polar stratospheric ozone loss on Southern Hemisphere stratospheric circulation and climate. *Atmospheric Chemistry and Physics*, *14*(24), 13705–13717. https://doi.org/10.5194/acp-14-13705-2014

Keeble, J., Hassler, B., Banerjee, A., Checa-Garcia, R., Chiodo, G., Davis, S., et al. (2021). Evaluating stratospheric ozone and water vapour changes in CMIP6 models from 1850 to 2100. *Atmospheric Chemistry and Physics*, *21*(6), 5015–5061. https://doi.org/10.5194/acp-21-5015-2021

Kelley, M., Schmidt, G. A., Nazarenko, L. S., Bauer, S. E., Ruedy, R., Russell, G. L., et al. (2020). GISS-E2.1: Configurations and climatology. *Journal of Advances in Modeling Earth Systems*, *12*(8), e2019MS002025. https://doi.org/10.1029/2019MS002025

Kim, Y.-H., Min, S.-K., Son, S.-W., & Choi, J. (2017). Attribution of the local Hadley cell widening in the Southern Hemisphere. *Geophysical Research Letters*, *44*(2), 1015–1024. https://doi.org/10.1002/2016GL072353

Kobayashi, S., Ota, Y., Harada, Y., Ebita, A., Moriya, M., Onoda, H., et al. (2015). The JRA-55 reanalysis: General specifications and basic characteristics [Dataset]. *Journal of the Meteorological Society of Japan. Series II*, *93*(1), 5–48. https://doi.org/10.2151/jmsj.2015-001

Kosaka, Y., Kobayashi, S., Harada, Y., Kobayashi, C., Naoe, H., Yoshimoto, K., et al. (2024). The JRA-3Q reanalysis [Dataset]. *Journal of the Meteorological Society of Japan. Series II*, *102*(1), 49–109. https://doi.org/10.2151/jmsj.2024-004

Kushner, P. J., Held, I. M., & Delworth, T. L. (2001). Southern Hemisphere atmospheric circulation response to global warming. *Journal of Climate*, *14*(10), 2238–2249. https://doi.org/10.1175/1520-0442(2001)014%3C0001:SHACRT%3E2.0.CO;2

Lachmy, O. (2022). The relation between the latitudinal shifts of midlatitude diabatic heating, eddy heat flux, and the eddy-driven jet in CMIP6 models. *Journal of Geophysical Research: Atmospheres*, *127*(16), e2022JD036556. https://doi.org/10.1029/2022JD036556

Lavergne, T., Sørensen, A. M., Kern, S., Tonboe, R., Notz, D., Aaboe, S., et al. (2019). Version 2 of the EUMETSAT OSI SAF and ESA CCI sea-ice concentration climate data records [Dataset]. *The Cryosphere*, *13*(1), 49–78. https://doi.org/10.5194/tc-13-49-2019

Lawrence, B. N., Bennett, V. L., Churchill, J., Juckes, M., Kershaw, P., Pascoe, S., et al. (2013). Storing and manipulating environmental big data with JASMIN [Software]. In *2013 IEEE International Conference on big data*, (pp. 68–75). https://doi.org/10.1109/BigData.2013.6691556

Lionello, P., D'Agostino, R., Ferreira, D., Nguyen, H., & Singh, M. S. (2024). The Hadley circulation in a changing climate. *Annals of the New York Academy of Sciences*, *1534*(1), 69–93. https://doi.org/10.1111/nyas.15114

Lovato, T., Peano, D., Butenschön, M., Materia, S., Iovino, D., Scoccimarro, E., et al. (2022). CMIP6 simulations with the CMCC Earth system model (CMCC-ESM2). *Journal of Advances in Modeling Earth Systems*, *14*(3), e2021MS002814. https://doi.org/10.1029/2021MS002814

Lurton, T., Balkanski, Y., Bastrikov, V., Bekki, S., Bopp, L., Braconnot, P., et al. (2020). Implementation of the CMIP6 forcing data in the IPSL-CM6A-LR model. *Journal of Advances in Modeling Earth Systems*, *12*(4), e2019MS001940. https://doi.org/10.1029/2019MS001940

Mackallah, C., Chamberlain, M. A., Law, R. M., Dix, M., Ziehn, T., Bi, D., et al. (2022). ACCESS datasets for CMIP6: Methodology and idealised experiments. *Journal of Southern Hemisphere Earth Systems Science*, *72*(2), 93–116. https://doi.org/10.1071/ES21031

Maher, N., Milinski, S., & Ludwig, R. (2021). Large ensemble climate model simulations: Introduction, overview, and future prospects for utilising multiple types of large ensemble. *Earth System Dynamics*, *12*(2), 401–418. https://doi.org/10.5194/esd-12-401-2021

Marshall, G. J. (2003). Trends in the southern annular mode from observations and reanalyses [Dataset]. *Journal of Climate*, *16*(24), 4134–4143. https://doi.org/10.1175/1520-0442(2003)016<4134:titsam>2.0.co;2

Mauritsen, T., Bader, J., Becker, T., Behrens, J., Bittner, M., Brokopf, R., et al. (2019). Developments in the MPI-M Earth system model version 1.2 (MPI-ESM1.2) and its response to increasing CO_2. *Journal of Advances in Modeling Earth Systems*, *11*(4), 998–1038. https://doi.org/10.1029/2018MS001400

McKay, R. C., Boschat, G., Rudeva, I., Pepler, A., Purich, A., Dowdy, A., et al. (2023). Can Southern Australian rainfall decline be explained? A review of possible drivers. *WIREs Climate Change*, *14*(2), e820. https://doi.org/10.1002/wcc.820

McLandress, C., Jonsson, A. I., Plummer, D. A., Reader, M. C., Scinocca, J. F., & Shepherd, T. G. (2010). Separating the dynamical effects of climate change and ozone depletion. Part I: Southern Hemisphere stratosphere. *Journal of Climate*, *23*(18), 5002–5020. https://doi.org/10.1175/2010JCLI3586.1

McLandress, C., Shepherd, T. G., Scinocca, J. F., Plummer, D. A., Sigmond, M., Jonsson, A. I., & Reader, M. C. (2011). Separating the dynamical effects of climate change and ozone depletion. Part II: Southern Hemisphere troposphere. *Journal of Climate*, *24*(6), 1850–1868. https://doi.org/10.1175/2010JCLI3958.1

Miller, R. L., Schmidt, G. A., Nazarenko, L. S., Bauer, S. E., Kelley, M., Ruedy, R., et al. (2021). CMIP6 historical simulations (1850–2014) with GISS-E2.1. *Journal of Advances in Modeling Earth Systems*, *13*(1), e2019MS002034. https://doi.org/10.1029/2019MS002034

Min, S.-K., & Son, S.-W. (2013). Multimodel attribution of the Southern Hemisphere Hadley cell widening: Major role of ozone depletion. *Journal of Geophysical Research: Atmospheres*, *118*(7), 3007–3015. https://doi.org/10.1002/jgrd.50232

Mindlin, J., Shepherd, T. G., Osman, M., Vera, C. S., & Kretschmer, M. (2025). Explaining and predicting the Southern Hemisphere eddy-driven jet. *Proceedings of the National Academy of Sciences*, *122*(29), e2500697122. https://doi.org/10.1073/pnas.2500697122

Morgenstern, O. (2021). The southern annular mode in 6th coupled model intercomparison project models. *Journal of Geophysical Research: Atmospheres*, *126*(5), e2020JD034161. https://doi.org/10.1029/2020JD034161

Nguyen, H., Lucas, C., Evans, A., Timbal, B., & Hanson, L. (2015). Expansion of the Southern Hemisphere Hadley cell in response to greenhouse gas forcing. *Journal of Climate*, *28*(20), 8067–8077. https://doi.org/10.1175/JCLI-D-15-0139.1

Parkinson, C. L. (2019). A 40-y record reveals gradual Antarctic sea ice increases followed by decreases at rates far exceeding the rates seen in the Arctic. *Proceedings of the National Academy of Sciences*, *116*(29), 14414–14423. https://doi.org/10.1073/pnas.1906556116

Perlwitz, J. (2011). Tug of war on the jet stream. *Nature Climate Change*, *1*(1), 29–31. https://doi.org/10.1038/nclimate1065

Polvani, L. M., Banerjee, A., Chemke, R., Doddridge, E. W., Ferreira, D., Gnanadesikan, A., et al. (2021). Interannual SAM modulation of Antarctic Sea ice extent does not account for its long-term trends, pointing to a limited role for ozone depletion. *Geophysical Research Letters*, *48*(21), e2021GL094871. https://doi.org/10.1029/2021GL094871

Polvani, L. M., Waugh, D. W., Correa, G. J. P., & Son, S.-W. (2011). Stratospheric ozone depletion: The main driver of twentieth-century atmospheric circulation changes in the Southern Hemisphere. *Journal of Climate*, *24*(3), 795–812. https://doi.org/10.1175/2010JCLI3772.1

Pope, J. O., Orr, A., Marshall, G. J., & Abraham, N. L. (2020). Non-additive response of the high-latitude Southern Hemisphere climate to aerosol forcing in a climate model with interactive chemistry. *Atmospheric Science Letters*, *21*(12), e1004. https://doi.org/10.1002/asl.1004

Purich, A., Arblaster, J. M., Boschat, G., Gillett, Z. E., Hobbs, W., Jucker, M., et al. (2026). Southern annular mode dynamics, projections and impacts in a changing climate. *Nature Reviews Earth and Environment*, *7*, 24–42. https://doi.org/10.1038/s43017-025-00746-y

Purich, A., Cowan, T., Min, S.-K., & Cai, W. (2013). Autumn precipitation trends over Southern Hemisphere midlatitudes as simulated by CMIP5 models. *Journal of Climate*, *26*(21), 8341–8356. https://doi.org/10.1175/JCLI-D-13-00007.1

Purich, A., & Doddridge, E. W. (2023). Record low Antarctic sea ice coverage indicates a new sea ice state. *Communications Earth and Environment*, *4*(1), 314. https://doi.org/10.1038/s43247-023-00961-9

Quaas, J., Jia, H., Smith, C., Albright, A. L., Aas, W., Bellouin, N., et al. (2022). Robust evidence for reversal of the trend in aerosol effective climate forcing. *Atmospheric Chemistry and Physics*, *22*(18), 12221–12239. https://doi.org/10.5194/acp-22-12221-2022

Roach, L. A., Dörr, J., Holmes, C. R., Massonnet, F., Blockley, E. W., Notz, D., et al. (2020). Antarctic sea ice area in CMIP6. *Geophysical Research Letters*, *47*(9), e2019GL086729. https://doi.org/10.1029/2019GL086729

Roach, L. A., Mankoff, K. D., Romanou, A., Blanchard-Wrigglesworth, E., Haine, T. W. N., Schmidt, & Gavin, A. (2023). Winds and meltwater together lead to southern ocean surface cooling and sea ice expansion. *Geophysical Research Letters*, *50*(24), e2023GL105948. https://doi.org/10.1029/2023gl105948

Rotstayn, L. D., Collier, M. A., Jeffrey, S. J., Kidston, J., Syktus, J. I., & Wong, K. K. (2013). Anthropogenic effects on the subtropical jet in the Southern Hemisphere: Aerosols versus long-lived greenhouse gases. *Environmental Research Letters*, *8*(1), 014030. https://doi.org/10.1088/1748-9326/8/1/014030

Saggioro, E., & Shepherd, T. G. (2019). Quantifying the timescale and strength of Southern Hemisphere intraseasonal stratosphere-troposphere coupling. *Geophysical Research Letters*, *46*(22), 13479–13487. https://doi.org/10.1029/2019GL084763

Salby, M., Titova, E., & Deschamps, L. (2011). Rebound of Antarctic ozone. *Geophysical Research Letters*, *38*(9). https://doi.org/10.1029/2011GL047266

Santer, B. D., Po-Chedley, S., Zhao, L., Zou, C.-Z., Fu, Q., Solomon, S., et al. (2023). Exceptional stratospheric contribution to human fingerprints on atmospheric temperature. *Proceedings of the National Academy of Sciences*, *120*(20), e2300758120. https://doi.org/10.1073/pnas.2300758120

Scaife, A. A., & Smith, D. (2018). A signal-to-noise paradox in climate science. *npj Climate and Atmospheric Science*, *1*(1), 28. https://doi.org/10.1038/s41612-018-0038-4

Schmidt, D. F., & Grise, K. M. (2017). The response of local precipitation and sea level pressure to Hadley cell expansion. *Geophysical Research Letters*, *44*(20), 10573–10582. https://doi.org/10.1002/2017GL075380

Schmidt, G. A., Romanou, A., Roach, L. A., Mankoff, K. D., Li, Q., Rye, C. D., et al. (2023). Anomalous meltwater from ice sheets and ice shelves is a historical forcing. *Geophysical Research Letters*, *50*(24), e2023GL106530. https://doi.org/10.1029/2023GL106530

Schneider, D. P., & Deser, C. (2018). Tropically driven and externally forced patterns of Antarctic sea ice change: Reconciling observed and modeled trends. *Climate Dynamics*, *50*(11), 4599–4618. https://doi.org/10.1007/s00382-017-3893-5

Seland, Ø., Bentsen, M., Olivié, D., Toniazzo, T., Gjermundsen, A., Graff, L. S., et al. (2020). Overview of the Norwegian Earth system model (NorESM2) and key climate response of CMIP6 DECK, historical, and scenario simulations. *Geoscientific Model Development*, *13*(12), 6165–6200. https://doi.org/10.5194/gmd-13-6165-2020

Seviour, W. J. M., Codron, F., Doddridge, E. W., Ferreira, D., Gnanadesikan, A., Kelley, M., et al. (2019). The southern ocean sea surface temperature response to ozone depletion: A multimodel comparison. *Journal of Climate*, *32*(16), 5107–5121. https://doi.org/10.1175/JCLI-D-19-0109.1

Shaw, T. A., Arblaster, J. M., Birner, T., Butler, A. H., Domeisen, D. I. V., Garfinkel, C. I., et al. (2024). Emerging climate change signals in atmospheric circulation. *AGU Advances*, *5*(6), e2024AV001297. https://doi.org/10.1029/2024AV001297

Shaw, T. A., Miyawaki, O., & Donohoe, A. (2022). Stormier Southern Hemisphere induced by topography and ocean circulation. *Proceedings of the National Academy of Sciences*, *119*(50), e2123512119. https://doi.org/10.1073/pnas.2123512119

Shi, J.-R., Talley, L. D., Xie, S.-P., Peng, Q., & Liu, W. (2021). Ocean warming and accelerating Southern Ocean zonal flow. *Nature Climate Change*, *11*(12), 1090–1097. https://doi.org/10.1038/s41558-021-01212-5

Shindell, D. T., & Schmidt, G. A. (2004). Southern Hemisphere climate response to ozone changes and greenhouse gas increases. *Geophysical Research Letters*, *31*(18). https://doi.org/10.1029/2004GL020724

Shiogama, H., Tatebe, H., Hayashi, M., Abe, M., Arai, M., Koyama, H., et al. (2023). MIROC6 large ensemble (MIROC6-LE): Experimental design and initial analyses. *Earth System Dynamics*, *14*(6), 1107–1124. https://doi.org/10.5194/esd-14-1107-2023

Sigmond, M., & Fyfe, J. C. (2010). Has the ozone hole contributed to increased Antarctic sea ice extent? *Geophysical Research Letters*, *37*(18). https://doi.org/10.1029/2010GL044301

Sigmond, M., & Fyfe, J. C. (2014). The Antarctic sea ice response to the ozone hole in climate models. *Journal of Climate*, *27*(3), 1336–1342. https://doi.org/10.1175/JCLI-D-13-00590.1

Sigmond, M., & Polvani, L. M. (2026). Large direct and indirect impacts of ozone-depleting substances on past Southern Hemisphere atmosphere-ocean trends. *npj Climate and Atmospheric Science*. https://doi.org/10.1038/s41612-026-01403-x

Sigmond, M., Reader, M. C., Fyfe, J. C., & Gillett, N. P. (2011). Drivers of past and future Southern Ocean change: Stratospheric ozone versus greenhouse gas impacts. *Geophysical Research Letters*, *38*(12). https://doi.org/10.1029/2011GL047120

Simpson, I. R., Rosenbloom, N., Danabasoglu, G., Deser, C., Yeager, S. G., McCluskey, C. S., et al. (2023). The CESM2 single-forcing large ensemble and comparison to CESM1: Implications for experimental design. *Journal of Climate*, *36*(17), 5687–5711. https://doi.org/10.1175/JCLI-D-22-0666.1

Simpson, I. R., Shaw, T. A., Ceppi, P., Clement, A. C., Fischer, E., Grise, K. M., et al. (2025). Confronting Earth system model trends with observations. *Science Advances*, *11*(11), eadt8035. https://doi.org/10.1126/sciadv.adt8035

Smith, D. M., Dunstone, N. J., Eade, R., Hardiman, S. C., Hermanson, L., Scaife, A. A., & Seabrook, M. (2025). Mitigation needed to avoid unprecedented multi-decadal North Atlantic oscillation magnitude. *Nature Climate Change*, *15*(4), 403–410. https://doi.org/10.1038/s41558-025-02277-2

Smith, D. M., Gillett, N. P., Simpson, I. R., Athanasiadis, P. J., Baehr, J., Bethke, I., et al. (2022). Attribution of multi-annual to decadal changes in the climate system: The large ensemble single forcing model intercomparison project (LESFMIP). *Frontiers in Climate*, *4*, 955414. https://doi.org/10.3389/fclim.2022.955414

Solomon, A., Polvani, L. M., Smith, K. L., & Abernathey, R. P. (2015). The impact of ozone depleting substances on the circulation, temperature, and salinity of the Southern Ocean: An attribution study with CESM1(WACCM). *Geophysical Research Letters*, *42*(13), 5547–5555. https://doi.org/10.1002/2015GL064744

Solomon, S., Ivy, D. J., Kinnison, D., Mills, M. J., Neely, R. R., & Schmidt, A. (2016). Emergence of healing in the Antarctic ozone layer. *Science*, *353*(6296), 269–274. https://doi.org/10.1126/science.aae0061

Son, S.-W., Han, B.-R., Garfinkel, C. I., Kim, S.-Y., Park, R., Abraham, N. L., et al. (2018). Tropospheric jet response to Antarctic ozone depletion: An update with chemistry-climate model initiative (CCMI) models. *Environmental Research Letters*, *13*(5), 054024. https://doi.org/10.1088/1748-9326/aabf21

Son, S.-W., Tandon, N. F., Polvani, L. M., & Waugh, D. W. (2009). Ozone hole and Southern Hemisphere climate change. *Geophysical Research Letters*, *36*(15), L15705. https://doi.org/10.1029/2009GL038671

Stephens, G. L., Kahn, B. H., & Richardson, M. (2016). The super greenhouse effect in a changing climate. *Journal of Climate*, *29*(15), 5469–5482. https://doi.org/10.1175/JCLI-D-15-0234.1

Suryawanshi, K., Jena, B., Bajish, C. C., & Anilkumar, N. (2023). Recent decline in Antarctic sea ice cover from 2016 to 2022: Insights from satellite observations, Argo floats, and model reanalysis. *Tellus*, *75*(1). https://doi.org/10.16993/tellusa.3222

Swart, N. C., Cole, J. N. S., Kharin, V. V., Lazare, M., Scinocca, J. F., Gillett, N. P., et al. (2019). The Canadian Earth system model version 5 (CanESM5.0.3). *Geoscientific Model Development*, *12*(11), 4823–4873. https://doi.org/10.5194/gmd-12-4823-2019

Swart, N. C., Gille, S. T., Fyfe, J. C., & Gillett, N. P. (2018). Recent Southern Ocean warming and freshening driven by greenhouse gas emissions and ozone depletion. *Nature Geoscience*, *11*(11), 836–841. https://doi.org/10.1038/s41561-018-0226-1

Thompson, D. W. J., & Solomon, S. (2002). Interpretation of recent Southern Hemisphere climate change. *Science*, *296*(5569), 895–899. https://doi.org/10.1126/science.1069270

Thompson, D. W. J., Solomon, S., Kushner, P. J., England, M. H., Grise, K. M., & Karoly, D. J. (2011). Signatures of the Antarctic ozone hole in Southern Hemisphere surface climate change. *Nature Geoscience*, *4*(11), 741–749. https://doi.org/10.1038/ngeo1296

Timbal, B., & Drosdowsky, W. (2013). The relationship between the decline of southeastern Australian rainfall and the strengthening of the subtropical ridge. *International Journal of Climatology*, *33*(4), 1021–1034. https://doi.org/10.1002/joc.3492

Varuolo-Clarke, A. M., Smerdon, J. E., Williams, A. P., & Seager, R. (2021). Gross discrepancies between observed and simulated twentieth-to-twenty-first-century precipitation trends in southeastern South America. *Journal of Climate*, *34*(15), 6441–6457. https://doi.org/10.1175/JCLI-D-20-0746.1

Vera, C. S., & Díaz, L. (2015). Anthropogenic influence on summer precipitation trends over South America in CMIP5 models. *International Journal of Climatology*, *35*(10), 3172–3177. https://doi.org/10.1002/joc.4153

Voldoire, A., Saint-Martin, D., Sénési, S., Decharme, B., Alias, A., Chevallier, M., et al. (2019). Evaluation of CMIP6 DECK experiments with CNRM-CM6-1. *Journal of Advances in Modeling Earth Systems*, *11*(7), 2177–2213. https://doi.org/10.1029/2019MS001683

Walz, R., Garny, H., & Birner, T. (2023). Stratospheric modulation of tropical upper-tropospheric warming-induced circulation changes in an idealized general circulation model. *Journal of the Atmospheric Sciences*, *80*(2), 611–631. https://doi.org/10.1175/JAS-D-21-0232.1

Wang, H., Xie, S.-P., Zheng, X.-T., Kosaka, Y., Xu, Y., & Geng, Y.-F. (2020). Dynamics of Southern Hemisphere atmospheric circulation response to anthropogenic aerosol forcing. *Geophysical Research Letters*, *47*(19), e2020GL089919. https://doi.org/10.1029/2020GL089919

Watanabe, M., Kang, S. M., Collins, M., Hwang, Y.-T., McGregor, S., & Stuecker, M. F. (2024). Possible shift in controls of the tropical Pacific surface warming pattern. *Nature*, *630*(8016), 315–324. https://doi.org/10.1038/s41586-024-07452-7

Waugh, D. W., Garfinkel, C. I., & Polvani, L. M. (2015). Drivers of the recent tropical expansion in the Southern Hemisphere: Changing SSTS or ozone depletion? *Journal of Climate*, *28*(16), 6581–6586. https://doi.org/10.1175/JCLI-D-15-0138.1

Wilcox, L. J., Charlton-Perez, A. J., & Gray, L. J. (2012). Trends in Austral jet position in ensembles of high- and low-top CMIP5 models. *Journal of Geophysical Research*, *117*(D13). https://doi.org/10.1029/2012JD017597

Wills, R. C. J., Dong, Y., Proistosecu, C., Armour, K. C., & Battisti, D. S. (2022). Systematic climate model biases in the large-scale patterns of recent sea-surface temperature and sea-level pressure change. *Geophysical Research Letters*, *49*(17), e2022GL100011. https://doi.org/10.1029/2022GL100011

Woollings, T., Drouard, M., O'Reilly, C. H., Sexton, D. M. H., & McSweeney, C. (2023). Trends in the atmospheric jet streams are emerging in observations and could be linked to tropical warming. *Communications Earth and Environment*, *4*(1), 125. https://doi.org/10.1038/s43247-023-00792-8

Xie, S.-P., Lu, B., & Xiang, B. (2013). Similar spatial patterns of climate responses to aerosol and greenhouse gas changes. *Nature Geoscience*, *6*(10), 828–832. https://doi.org/10.1038/ngeo1931

Yang, D., Arblaster, J. M., Meehl, G. A., England, M. H., Lim, E.-P., Bates, S., & Rosenbloom, N. (2020). Role of tropical variability in driving decadal shifts in the Southern Hemisphere summertime eddy-driven jet. *Journal of Climate*, *33*(13), 5445–5463. https://doi.org/10.1175/JCLI-D-19-0604.1

Yeager, S. G., Chang, P., Danabasoglu, G., Rosenbloom, N., Zhang, Q., Castruccio, F. S., et al. (2023). Reduced Southern Ocean warming enhances global skill and signal-to-noise in an eddy-resolving decadal prediction system. *npj Climate and Atmospheric Science*, *6*(1), 107. https://doi.org/10.1038/s41612-023-00434-y

Zambri, B., Solomon, S., Thompson, D. W. J., & Fu, Q. (2021). Emergence of Southern Hemisphere stratospheric circulation changes in response to ozone recovery. *Nature Geoscience*, *14*(9), 638–644. https://doi.org/10.1038/s41561-021-00803-3

Zhang, H., Delworth, T. L., Zeng, F., Vecchi, G., Paffendorf, K., & Jia, L. (2016). Detection, attribution, and projection of regional rainfall changes on (multi-) decadal time scales: A focus on southeastern South America. *Journal of Climate*, *29*(23), 8515–8534. https://doi.org/10.1175/JCLI-D-16-0287.1

Zheng, F. (2024). Slowing down of the summer Southern Hemisphere annular mode trend against the background of ozone recovery. *Atmospheric and Oceanic Science Letters*, *17*(1), 100375. https://doi.org/10.1016/j.aosl.2023.100375

Ziehn, T., Chamberlain, M. A., Law, R. M., Lenton, A., Bodman, R. W., Dix, M., et al. (2020). The Australian Earth system model: ACCESS-ESM1.5. *Journal of Southern Hemisphere Earth Systems Science*, *70*(1), 193–214. https://doi.org/10.1071/ES19035